Analysis of Subtidal Coastal Sea Level Fluctuations Using Wavelets

Donald B. Percival* and Harold O. Mofjeld†

An understanding of subtidal coastal sea level fluctuations is important both because they impact the effect of tsunamis and other destructive events on human developments and because many physical and biological processes within coastal ecosystems are very sensitive to these fluctuations. We analyze a time series of subtidal fluctuations at Crescent City, California, during 1980–91 using the maximal overlap discrete wavelet transform (MODWT). Our analysis shows that these fluctuations have seasonally dependent variability over scales of 32 day and less. We show how this nonstationary behavior can be succinctly characterized in terms of the MODWT, and we indicate how this characterization can be used to improve forecasting schemes for inundation during tsunamis and storm surges. Because the standard tools in time series analysis are best suited for stationary processes and because our case study demonstrates that MODWT analysis is useful for characterizing certain nonstationary processes, we provide pseudo-code and enough background information so that data analysts in other disciplines can readily apply MODWT analysis to their time series.

Key Words: Coastal sea level variability; Discrete wavelet transform; Natural hazards; Time series analysis; Tsunamis

* Senior Mathematician, Applied Physics Laboratory, University of Washington, Seattle, WA 98195; Research Scientist, MathSoft, Inc., 1700 Westlake Avenue North, Seattle, WA 98109; Affiliate Associate Professor, Department of Statistics, University of Washington, Seattle, WA 98195

† Research Oceanographer, Pacific Marine Environmental Laboratory, National Oceanic and Atmospheric Administration, Seattle, WA 98115; Affiliate Associate Professor, School of Oceanography, University of Washington, Seattle, WA 98195

1. INTRODUCTION

Sea level fluctuations strongly influence the impacts that the ocean has on both human activities and coastal ecosystems within the coastal zone. For example, these fluctuations help determine the levels of inundation caused by tsunamis, storm surges and high waves. Many physical and biological processes are very sensitive to short- and long-term fluctuations in sea level. The effects of sea level fluctuations depend on their amplitudes, their duration of time and when they occur during the year. In general, sea level fluctuations are due to the astronomical tides, runoff from rivers, and the response of the coastal ocean to meteorological forcing. On longer time scales, they respond to varying ocean currents, the seasonal heating and cooling of the adjacent ocean, and interannual phenomena such as the El Niño/Southern Oscillation cycle in the Equatorial Pacific Ocean and variations in the Pacific–North American pattern in the atmosphere.

The astronomical tides usually dominate sea level fluctuations at the coast. These tides are highly predictable because they are well-modeled as stationary harmonic processes with precise frequencies, especially near one and two cycles per day (Pugh, 1987). In contrast, subtidal fluctuations occur over a very broad range of longer time scales and are highly non-stationary. While the amplitudes of subtidal fluctuations are often less than those of tides, they can be large enough to influence the impacts of tsunamis and other coastal hazards. The subtidal fluctuations are also of scientific interest because they provide considerable insight into the ways in which the coastal ocean responds to atmospheric forcing and currents. Background material on these fluctuations can be found in, e.g., Pattullo *et al.* (1955), Roden (1960), Chelton and Davis (1982), Halliwell and Allen (1984), Denbo and Allen (1987), Enfield (1987), Spillane *et al.* (1987), Strub *et al.* (1987a, b), Strub and James (1988), Hickey (1989) and Roden (1989).

In this paper, we demonstrate that wavelet analysis based on the maximal overlap discrete wavelet transform (MODWT) is an effective technique for quantifying the nonstationary characteristics of subtidal sea level fluctuations as measured by the tide gauge at Crescent City, California. This site is of particular interest because Crescent City has a well-documented history of tsunami inundation in which the maximum heights depend strongly of the heights of subtidal sea level (Petrauskas and Borgman, 1971; Lander and Lockridge, 1989; Mofjeld *et al.*, 1997a). The ocean near Crescent City is also subject to the highest seasonal wind forcing along the U.S. West Coast (Strub *et al.*, 1987b). The period of interest is 1980–1991, which includes the major 1982–83 El Niño/Southern Oscillation event and several other interannual events. The primary scientific purpose of this paper is to characterize the subtidal sea level fluctuations at Crescent City as they relate to coastal hazards. These characterizations can then be used to improve maps and forecasts of coastal inundation (Mofjeld *et al.*, 1997a, b).

The MODWT of a time series leads to two types of analyses. The first is an additive decomposition known as multiresolution analysis, which breaks up the series into a number of "details" and a single "smooth." Each detail is a time series describing variations at a particular time scale, while the smooth describes the low frequency variations. We use the details from the Crescent City series to study its temporal behavior at the synoptic (1–10 days) and intraseasonal scales and use the smooth to study its seasonal and longer scale fluctuations. Stacked plots of the details and smooth provide an effective means of exploring the relationships between sea level fluctuations at different time scales.

The second type of analysis decomposes the sample variance of the time series both across different scales and over time. The decomposition across time is facilitated by our use of a compactly supported "least asymmetric" (LA) wavelet filter due to Daubechies (1992), which helps align events in the analysis with events in the original series. Because time-dependent events at various scales are properly localized, MODWT analysis of variance is particularly useful for time series with nonstationary characteristics, such as exhibited by the subtidal fluctuations at Crescent City. For these fluctuations, MODWT analysis of variance suggests a simple model for annual cycles of scale-dependent variations in variance that can be useful in operational forecasting.

Following this introduction, we devote two sections to summarizing wavelet methodology. Section 2 describes the orthonormal discrete wavelet transform (DWT). This section provides essential background for the MODWT (Section 3), which is used to analyze the subtidal sea level series at Crescent City. Section 4 presents the results for the MODWT analysis, while Section 5 interprets and discusses the implications of these results and the advantages of the MODWT approach over more traditional methods. Section 6 summarizes the conclusions of the paper. We have also included appendices containing pseudo-code and proofs of the basic properties of the MODWT. Enough detail is provided so that practitioners can apply

MODWT analysis in other problem areas.

2. THE DISCRETE WAVELET TRANSFORM

In this section we summarize the discrete wavelet transform (DWT) and DWT-based multiresolution and variance analyses. Let $\mathbf{X}$ be a column vector containing a sequence $X_0, X_1, \ldots, X_{N-1}$ of N observations of a real-valued time series. We assume that the observation X_t was collected at time $t\,\Delta t$, where Δt is the time interval between adjacent observations (for example, $\Delta t = 1/2$ day for the subtidal sea level series at Crescent City). In this section we also assume that the sample size N is an integer multiple of 2^J, where J is a positive integer.

The DWT of level J is an orthonormal transform of $\mathbf{X}$ defined by $\mathbf{W} = \mathcal{W}\mathbf{X}$, where $\mathbf{W}$ is a column vector of length N, and $\mathcal{W}$ is an $N \times N$ real-valued matrix satisfying $\mathcal{W}^T\mathcal{W} = I$. The vector $\mathbf{W}$ contains the transform coefficients, and its first $N - N/2^J$ elements and last $N/2^J$ elements are called, respectively, wavelet and scaling coefficients. Explicit construction of $\mathcal{W}$ is outlined in Section 2.1. Qualitatively, if we let $\tau_j \equiv 2^{j-1}$, each wavelet coefficient is associated with changes on a particular scale $\tau_j\,\Delta t$ at a localized set of times; i.e., a wavelet coefficient tells us how much a weighted average changes from a particular time period of effective length $\tau_j\,\Delta t$ to the next. There are exactly $N/2^j$ wavelet coefficients associated with scale $\tau_j\,\Delta t$, where $j = 1, \ldots, J$. The $N/2^J$ scaling coefficients are associated with variations on scales $\tau_{J+1}\,\Delta t$ and higher; i.e., a scaling coefficient is a weighted average with bandwidth $\tau_{J+1}\,\Delta t$ over a particular time period of effective length $\tau_{J+1}\,\Delta t$. Background material on wavelets supporting this qualitative description and supplementing the mathematical development in the next three subsections can be found in, e.g., Mallat (1989), Daubechies (1992), Press *et al.* (1992), Meyer (1993), Strang (1993), Newland (1993), Nason and Silverman (1994), Percival and Guttorp (1994), Percival (1995), McCoy and Walden (1996) and Lindsay *et al.* (1996).

2.1 Construction of the DWT

The DWT matrix $\mathcal{W}$ is constructed based entirely upon a wavelet filter $h_{1,0}, \ldots, h_{1,L_1-1}$ of even length L_1 (Mallat, 1989; Daubechies, 1992, Ch. 6). For convenience we assume $L_1 \leq N$. By definition, this filter sums to zero, has unit norm and is orthogonal to its even shifts:

$$\sum_{n=0}^{L_1-1-2l} h_{1,n}h_{1,n+2l} = \begin{cases} 1, & l = 0; \\ 0, & l = 1, 2, \ldots, (L_1-2)/2. \end{cases} \quad (1)$$

The filter $h_{1,n}$ is associated with the scale $\Delta t = \tau_1\,\Delta t$ and is approximately a highpass filter with a pass-band given by the interval of frequencies $[1/(4\,\Delta t), 1/(2\,\Delta t)]$. To define the wavelet filter $h_{j,n}$ for higher scales $\tau_j\,\Delta t$, let

$$H_{1,k} \equiv \sum_{n=0}^{N-1} h_{1,n} e^{-i2\pi nk/N}, \qquad k = 0, \ldots, N-1,$$

be the discrete Fourier transform (DFT) of the wavelet filter padded with $N - L_1$ zeros. Let $g_{1,n}$ be the corresponding scaling filter, which is defined as

$$g_{1,n} \equiv (-1)^{n+1} h_{1,L_1-1-n}, \qquad n = 0, \ldots, L_1-1. \quad (2)$$

Let $G_{1,k}$ denote the DFT of the zero-padded scaling filter. The higher order wavelet filters are defined as

$$h_{j,n} \equiv \frac{1}{N}\sum_{k=0}^{N-1} H_{j,k} e^{i2\pi nk/N}, \text{ where } H_{j,k} \equiv H_{1,2^{j-1}k \bmod N} \prod_{l=0}^{j-2} G_{1,2^l k \bmod N}. \quad (3)$$

Elements $h_{j,L_j}, h_{j,L_j+1}, \ldots, h_{j,N-1}$ of this real-valued filter will be equal to zero when $L_j \equiv (2^j-1)(L_1-1)+1 < N$. The filter $h_{j,n}$ is approximately a bandpass filter with a pass-band given by $[1/(2^{j+1}\Delta t), 1/(2^j\Delta t)]$. Finally, we define the Jth order scaling filter as

$$g_{J,n} \equiv \frac{1}{N}\sum_{k=0}^{N-1} G_{J,k} e^{i2\pi nk/N}, \text{ where } G_{J,k} \equiv \prod_{l=0}^{J-1} G_{1,2^l k \bmod N}. \quad (4)$$

The filter $g_{J,n}$ is approximately a lowpass filter with pass-band $[0, 1/(2^{J+1}\Delta t)]$.

The first $N - N/2^J$ rows of the matrix $\mathcal{W}$ contain shifted versions of the wavelet filters $h_{j,m}$, $j = 1, 2, \ldots, J$. To be explicit, let the column vector

$$\mathbf{h}_j \equiv [\, h_{j,0}, \quad h_{j,N-1}, \quad h_{j,N-2}, \quad \ldots, \quad h_{j,2}, \quad h_{j,1} \,]^T \tag{5}$$

contain the elements of the filter $h_{j,n}$. Let $\mathcal{T}$ be the $N \times N$ matrix that circularly shifts $\mathbf{h}_j$ by one unit:

$$\mathcal{T}\mathbf{h}_j = [\, h_{j,1}, \quad h_{j,0}, \quad h_{j,N-1}, \quad \ldots, \quad h_{j,3}, \quad h_{j,2} \,]^T .$$

Let $\mathcal{T}^2\mathbf{h}_j \equiv \mathcal{T}\mathcal{T}\mathbf{h}_j$ and so forth. With $j = 1, \ldots, J$, the matrix $\mathcal{W}^T$ has $N/2^j$ columns associated with scale $\tau_j\,\Delta t$, namely, $\mathcal{T}^{2^j k-1}\mathbf{h}_j$, $k = 1, \ldots, N/2^j$, where k is a location index. The first $M/2$ columns in $\mathcal{W}^T$ are $\mathcal{T}^{2k-1}\mathbf{h}_1$, $k = 1, \ldots, N/2$; the next $N/4$ columns are the circularly shifted versions of $\mathbf{h}_2$; and so forth, until we come to columns containing circularly shifted versions of $\mathbf{h}_J$, namely, $\mathcal{T}^{2^J k-1}\mathbf{h}_J$, $k = 1, \ldots, N/2^J$. The $N/2^j$ wavelet coefficients associated with scale $\tau_j\,\Delta t$ can be interpreted as circularly filtering $\mathbf{X}$ using the filter $\mathbf{h}_j$ and then subsampling every 2^jth value of the filter output (this is called downsampling in the engineering literature). Likewise, the last $N/2^J$ columns of $\mathcal{W}^T$ contain shifted versions of the Jth order scaling filter $g_{J,n}$, namely, $\mathcal{T}^{2^J k-1}\mathbf{g}_J$, $k = 1, \ldots, N/2^J$, where

$$\mathbf{g}_J \equiv [\, g_{J,0}, \quad g_{J,N-1}, \quad g_{J,N-2}, \quad \ldots, \quad g_{J,2}, \quad g_{J,1} \,]^T . \tag{6}$$

Again, the $N/2^J$ scaling coefficients can be interpreted as taking every 2^Jth value obtained by circularly filtering $\mathbf{X}$ with $\mathbf{g}_J$. A proof that $\mathcal{W}$ so constructed is orthonormal is given in e.g., Mallat (1989), Daubechies (1992) and Newland (1993).

2.2 Multiresolution Analysis via the DWT

Because the DWT matrix $\mathcal{W}$ is orthonormal by construction, we can reconstruct (synthesize) our time series from its wavelet coefficients $\mathbf{W}$ using $\mathbf{X} = \mathcal{W}^T\mathbf{W}$. The idea behind multiresolution analysis is to express $\mathcal{W}^T\mathbf{W}$ as the sum of several new series, each of which is related to variations in $\mathbf{X}$ at a certain scale. To do so, we decompose the vector $\mathbf{W}$ into $J + 1$ subvectors, namely, $\mathbf{W}_j$, $j = 1, \ldots, J$, and $\mathbf{V}_J$. The subvector $\mathbf{W}_j$ contains all of the wavelet coefficients for scale τ_j and hence is a column vector with $N/2^j$ elements; the subvector $\mathbf{V}_J$ contains the $N/2^J$ scaling coefficients. We can then write $\mathbf{W} = [\, \mathbf{W}_1^T \quad \mathbf{W}_2^T \quad \cdots \quad \mathbf{W}_J^T \quad \mathbf{V}_J^T \,]^T$. Next we partition the columns of $\mathcal{W}^T$ commensurate with the partitioning of $\mathbf{W}$ to obtain

$$\mathcal{W}^T = [\, \mathcal{W}_1 \quad \mathcal{W}_2 \quad \cdots \quad \mathcal{W}_J \quad \mathcal{V}_J \,],$$

where $\mathcal{W}_j$ is an $N \times N/2^j$ matrix, while $\mathcal{V}_J$ is an $N \times N/2^J$ matrix. Note that $\mathbf{W}_j = \mathcal{W}_j^T\mathbf{X}$ and $\mathbf{V}_J = \mathcal{V}_J^T\mathbf{X}$. We can now write

$$\mathbf{X} = \mathcal{W}^T\mathbf{W} = \sum_{j=1}^{J} \mathcal{W}_j\mathbf{W}_j + \mathcal{V}_J\mathbf{V}_J \equiv \sum_{j=1}^{J} \mathcal{D}_j + \mathcal{S}_J \tag{7}$$

where $\mathcal{D}_j \equiv \mathcal{W}_j\mathbf{W}_j$ for $j = 1, \ldots, J$ is an N dimensional column vector whose elements are associated with changes at the scale τ_j, and $\mathcal{S}_J \equiv \mathcal{V}_J\mathbf{V}_J$ is a similar vector with elements associated with variations at scales τ_{J+1} and higher; i.e., $\mathcal{D}_j = \mathcal{W}_j\mathcal{W}_j^T\mathbf{X}$ is the portion of the synthesis $\mathbf{X} = \mathcal{W}^T\mathbf{W}$ attributable to changes over the scale $\tau_j\,\Delta t$, while $\mathcal{S}_J = \mathcal{V}_J\mathcal{V}_J^T\mathbf{X}$ is the portion attributable to variations at scales τ_{J+1} and higher. We refer to $\mathcal{D}_j$ and $\mathcal{S}_J$ as, respectively, the jth order *detail* and the Jth order *smooth* for $\mathbf{X}$, and the above decomposition defines a Jth order multiresolution analysis of $\mathbf{X}$.

2.3 Analysis of Variance via the DWT

Orthonormality of $\mathcal{W}$ implies that

$$\|\mathbf{W}\|^2 = \|\mathbf{X}\|^2 \equiv \sum_{t=0}^{N-1} X_t^2.$$

Decomposing $\mathbf{W}$ into subvectors $\mathbf{W}_j$ and $\mathbf{V}_J$ yields

$$\|\mathbf{X}\|^2 = \sum_{j=1}^{J} \|\mathbf{W}_j\|^2 + \|\mathbf{V}_J\|^2, \tag{8}$$

so $\|\mathbf{W}_j\|^2$ represents the contribution to the squared norm of $\mathbf{X}$ due to changes at scale τ_j, while $\|\mathbf{V}_J\|^2$ represents the contribution due to variations at scales τ_{J+1} and higher. We can also write

$$\hat{\sigma}_X^2 \equiv \frac{1}{N}\sum_{t=0}^{N-1}\left(X_t - \overline{X}\right)^2 = \frac{1}{N}\|\mathbf{W}\|^2 - \overline{X}^2 = \frac{1}{N}\sum_{j=1}^{J}\|\mathbf{W}_j\|^2 + \frac{1}{N}\|\mathbf{V}_J\|^2 - \overline{X}^2,$$

where $\hat{\sigma}_X^2$ is the sample variance of $\mathbf{X}$, and $\overline{X} = \frac{1}{N}\sum X_t$ is its sample mean. Hence $\|\mathbf{W}_j\|^2/N$ is the contribution to the sample variance of $\mathbf{X}$ due to changes at scale τ_j. Furthermore, the orthonormality of $\mathcal{W}$ implies that $\|\mathcal{D}_j\|^2 = \|\mathbf{W}_j\|^2$ and $\|\mathcal{S}_J\|^2 = \|\mathbf{V}_J\|^2$. Hence we have

$$\hat{\sigma}_X^2 = \frac{1}{N}\sum_{j=1}^{J}\|\mathcal{D}_j\|^2 + \frac{1}{N}\|\mathcal{S}_J\|^2 - \overline{X}^2,$$

where $\|\mathcal{D}_j\|^2/N$ can be interpreted to be the sample variance of the N elements of $\mathcal{D}_j$, while $\frac{1}{N}\|\mathcal{S}_J\|^2 - \overline{X}^2$ is the sample variance of the N elements of $\mathcal{S}_J$ (the results of McCoy and Walden, 1996, can be used to deduce that the sample mean of the N elements of $\mathcal{S}_J$ is equal to $\overline{X}$).

3. THE MAXIMAL OVERLAP DISCRETE WAVELET TRANSFORM

Here we describe a modified version of the discrete wavelet transform called the maximal overlap DWT (MODWT). The name comes from the literature on the Allan variance (a well-known measure of the performance of atomic clocks), in conjunction with which the MODWT based upon the Haar wavelet filter has been used for over two decades (see Greenhall, 1991, and Percival and Guttorp, 1994). Essentially the same transform has been discussed in the wavelet literature in the context of infinite sequences under the name "undecimated DWT" (Shensa, 1992), and in the context of "power of two" sequences under the names "stationary DWT" (Nason and Silverman, 1995), "translation invariant DWT" (Coifman and Donoho, 1995; Liang and Parks, 1996) and "time invariant DWT" (Pesquet *et al.*, 1996). The MODWT of level J for a time series $\mathbf{X}$ is a highly redundant nonorthogonal transform yielding the column vectors $\widetilde{\mathbf{W}}_1$, $\widetilde{\mathbf{W}}_2$, …, $\widetilde{\mathbf{W}}_J$ and $\widetilde{\mathbf{V}}_J$, each with dimension N. The vector $\widetilde{\mathbf{W}}_j$ contains the MODWT wavelet coefficients associated with changes in $\mathbf{X}$ on a scale of $\tau_j\,\Delta t$, while $\widetilde{\mathbf{V}}_J$ contains the MODWT scaling coefficients associated with variations at scales $\tau_{J+1}\,\Delta t$ and higher.

There are four important properties that distinguish the MODWT from the DWT:

[1] While the DWT of level J restricts the sample size to an integer multiple of 2^J, the MODWT of level J is well defined for any sample size N (for convenience, however, we again assume that N is at least as large as the length L_1 of the wavelet filter). When N is an integer multiple of 2^J, the DWT can be computed using $O(N)$ multiplications, whereas the corresponding MODWT requires $O(N \log_2 N)$ multiplications. There is thus a computational price to pay for using the MODWT, but its computational burden is the same as the widely used fast Fourier transform algorithm and hence is usually quite acceptable.

[2] As is true for the DWT, the MODWT can be used to form a multiresolution analysis. In contrast to the usual DWT, both the MODWT wavelet and scaling coefficients and multiresolution analysis are shift invariant in the sense that circularly shifting the time series by any amount will circularly shift by a corresponding amount the MODWT wavelet and scaling coefficients, details and smooths.

[3] In contrast to the DWT details and smooths, the MODWT details and smooths are associated with zero phase filters, thus making it possible to meaningfully line up features in a multiresolution analysis with the original time series. The importance of this property is illustrated in Section 5.3.

[4] As is true for the DWT, the MODWT can be used to form an analysis of variance based upon the wavelet and scaling coefficients. Under a stationarity assumption on the wavelet coefficients, the MODWT yields an estimator of the variance of the wavelet coefficients that is statistically more efficient than the corresponding estimator based on the DWT.

Property [2] is discussed in all the papers referenced above, while property [4] is discussed in Percival (1995) and Lindsay *et al.* (1996). Properties [1] and [3] are discussed in the subsections below. Section 3.1 discusses explicit construction of the $\widetilde{\mathbf{W}}_j$'s and $\widetilde{\mathbf{V}}_J$, while Sections 3.2 and 3.3 discuss how to form, respectively, a multiresolution analysis and an analysis of variance based upon the MODWT. Appendix 1 gives pseudo-code for computing the MODWT, while Appendix 2 contains proofs of two key properties of the MODWT.

3.1 Construction of the MODWT

The MODWT wavelet and scaling vectors are constructed using the rescaled filter vectors $\tilde{\mathbf{h}}_j \equiv \mathbf{h}_j/2^{j/2}$, $j = 1, \ldots, J$, and $\tilde{\mathbf{g}}_J \equiv \mathbf{g}_J/2^{J/2}$, where $\mathbf{h}_j$ and $\mathbf{g}_J$ are defined in Equations (5) and (6). The elements $\widetilde{W}_{j,k}$ of $\widetilde{\mathbf{W}}_j$ are given by $\mathbf{X}^T\mathcal{T}^k\tilde{\mathbf{h}}_j$, $k = 0, \ldots, N-1$, while the elements $\widetilde{V}_{J,k}$ of $\widetilde{\mathbf{V}}_J$ are given by $\mathbf{X}^T\mathcal{T}^k\tilde{\mathbf{g}}_J$. The N wavelet and scaling coefficients for the MODWT can thus be interpreted as circularly filtering $\mathbf{X}$ using the filters $\tilde{\mathbf{h}}_j$ and $\tilde{\mathbf{g}}_J$ with *no* subsampling. In fact, a comparison of the definitions of the DWT and MODWT shows that, if N were an integer multiple of 2^J so that we could use the DWT, we can recover the DWT from the MODWT by subsampling and rescaling the latter: the elements $W_{j,k}$ and $V_{J,k}$ of $\mathbf{W}_j$ and $\mathbf{V}_J$ are equal to, respectively, $2^{j/2}\widetilde{W}_{j,2^j(k+1)-1}$, $k = 0, \ldots, N/2^j - 1$, and $2^{J/2}\widetilde{V}_{J,2^J(k+1)-1}$, $k = 0, \ldots, N/2^J - 1$.

3.2 Multiresolution Analysis via the MODWT

Consider the circular filter of length N whose DFT is given by the complex conjugate of $H_{j,k}/2^{j/2}$. Because

$$\frac{1}{2^{j/2}}\sum_{n=0}^{N-1} h_{j,n}e^{i2\pi nk/N} = \frac{1}{2^{j/2}}\sum_{n=0}^{N-1} h_{j,N-n \bmod N}e^{-i2\pi nk/N},$$

it follows that the filter vector corresponding to the complex conjugate of $H_{j,k}/2^{j/2}$ is given by

$$\tilde{\mathbf{h}}_j^* \equiv \left[\, h_{j,0}, \quad h_{j,1}, \quad h_{j,2}, \quad \ldots, \quad h_{j,N-2}, \quad h_{j,N-1}\right]^T/2^{j/2}.$$

Similarly, the filter vector corresponding to the complex conjugate of $G_{J,k}/2^J$ is given by

$$\tilde{\mathbf{g}}_J^* \equiv \left[\, g_{J,0}, \quad g_{J,1}, \quad g_{J,2}, \quad \ldots, \quad g_{J,N-2}, \quad g_{J,N-1}\right]^T/2^{J/2}.$$

The elements of the jth order maximal-overlap detail $\widetilde{\mathcal{D}}_j$ are defined to be $\widetilde{\mathbf{W}}_j^T\mathcal{T}^k\tilde{\mathbf{h}}_j^*$, $k = 0, \ldots, N-1$; likewise, the elements of the Jth order maximal-overlap smooth $\widetilde{\mathcal{S}}_J$ are defined to be $\widetilde{\mathbf{V}}_J^T\mathcal{T}^k\tilde{\mathbf{g}}_J^*$, $k = 0, \ldots, N-1$. With these definitions, it is shown in Appendix 2 that

$$\mathbf{X} = \sum_{j=1}^{J}\widetilde{\mathcal{D}}_j + \widetilde{\mathcal{S}}_J, \tag{9}$$

which constitutes a MODWT multiresolution analysis analogous to Equation (7) for the DWT. Appendix 1 describes how to compute $\widetilde{\mathcal{D}}_j$ and $\widetilde{\mathcal{S}}_J$ efficiently.

Since $\widetilde{\mathcal{D}}_j$ is obtained by circularly filtering $\mathbf{X}$ with $\mathbf{h}_j$ to yield $\widetilde{\mathbf{W}}_j$ and then circularly filtering $\widetilde{\mathbf{W}}_j$ with $\mathbf{h}_j^*$, we can equivalently obtain $\widetilde{\mathcal{D}}_j$ by circularly filtering $\mathbf{X}$ with a single filter whose DFT is given by $|H_{j,k}|^2/2^j$. Because this DFT is real-valued and nonnegative, the equivalent filter is said to have zero phase (see, e.g, Hamming, 1989, p. 252). The zero phase property is important because it allows us to meaningfully line up events in the details and smooth with events in the original time series. By contrast, the DWT details and smooth are not produced by zero phase filters, which we demonstrate in Section 5.3 can lead to misalignment of events with respect to the original time series $\mathbf{X}$. A similar argument allows us to claim that $\widetilde{\mathcal{S}}_J$ is the output from a zero phase filter with DFT given by $|G_{J,k}|^2/2^J$.

3.3 Analysis of Variance via the MODWT

As shown in Appendix 2, we can write

$$\|\mathbf{X}\|^2 = \sum_{j=1}^{J} \|\widetilde{\mathbf{W}}_j\|^2 + \|\widetilde{\mathbf{V}}_J\|^2 \tag{10}$$

(cf. Equation (8) for the DWT). The above is the basic result needed to define a MODWT-based analysis of variance, allowing us to partition the sample variance of the series on a scale by scale basis. Examples of the use of the MODWT for the analysis of variance of time series are given in Percival and Guttorp (1994), Percival (1995) and Lindsay *et al.* (1996).

It is important to point out that, whereas we have the relationship $\|\mathbf{W}_j\|^2 = \|\mathcal{D}_j\|^2$ for the usual DWT, we do *not* in general have equality between $\|\widetilde{\mathbf{W}}_j\|^2$ and $\|\widetilde{\mathcal{D}}_j\|^2$. Hence we cannot use the MODWT details and smooth for analysis of variance, which is unfortunate because their zero phase properties would allow us to meaningfully partition $\|\widetilde{\mathcal{D}}_j\|^2$ with respect to time. Daubechies (1992, Theorem 8.1.4) demonstrates that wavelet and scaling filters of finite length L_1 cannot have zero phase exactly; however, Daubechies (1992, Section 8.1.1) derives a class of "least asymmetric" (LA) wavelets that are close approximations to zero phase filters if the filter outputs $\widetilde{\mathbf{W}}_j$ and $\widetilde{\mathbf{V}}_J$ are circularly shifted appropriately. We refer to members of this class as LA(L_1) wavelets, where $L_1 = 8, 10, \ldots, 18$ or 20 identifies a particular wavelet by its number of nonzero coefficients. Circular shifting yields $\mathcal{T}^{\nu_j^{(H)}}\widetilde{\mathbf{W}}_j$ and $\mathcal{T}^{\nu_J^{(G)}}\widetilde{\mathbf{V}}_J$, where the shifts $\nu_j^{(H)}$ and $\nu_J^{(G)}$ are given in Appendix 3. Since $\|\mathcal{T}^{\nu_j^{(H)}}\widetilde{\mathbf{W}}_j\|^2 = \|\widetilde{\mathbf{W}}_j\|^2$ and since $\mathcal{T}^{\nu_j^{(H)}}\widetilde{\mathbf{W}}_j$ is an approximation to a zero phase filtering of $\mathbf{X}$, the portion $\|\mathcal{T}^{\nu_j^{(H)}}\widetilde{\mathbf{W}}_j\|^2$ of the analysis of variance associated with scale τ_j can be further decomposed across the time. An example of this procedure is given in the next section.

4. ANALYSIS OF CRESCENT CITY SUBTIDAL SEA LEVELS

In this section we use MODWT multiresolution analysis and analysis of variance to study a time series of subtidal sea level fluctuations for Crescent City, which is located at latitude 41° 45′ N and longitude 124° 11′ W on the open coast of Northern California. Inside its harbor, a permanent tide gauge is maintained by the National Ocean Service (NOS). The gauge measures water levels every 6 minutes within a stilling well that consists of a vertical tube with small openings near the bottom. These openings admit the tides and lower frequency fluctuations into the well but suppress the higher frequency fluctuations due to wind waves and swell. Periodic leveling surveys ensure that the reference level of the gauge remains constant relative to the surrounding land. The time series used in this paper was collected from January 1980 to December 1991 and was reduced to hourly data by subsampling. The hourly data contain a two-week gap in summer 1990 (filled with predicted tides and a local mean) and a few shorter gaps (filled by interpolation). Subtidal fluctuations were extracted from the hourly data by low-pass filtering to remove astronomical tides at diurnal and higher frequencies (we used a Kaiser filter with a half-power (3 dB down) point at a period of 1.82 days and with $< 1\%$ power attenuation at periods > 2.68 days – see Hamming, 1989, for details). The filtered series was then resampling every 1/2 day, yielding a Nyquist frequency of one cycle per day. The resulting time series $\mathbf{X}$ is plotted at the bottom of Figure 1.

Previous studies of subtidal sea level fluctuations at Crescent City are given in Roden (1960), Denbo and Allen (1987), Spillane *et al.* (1987) and Strub *et al.* (1987b). These studies indicate that the subtidal fluctuations are predominantly forced by the atmosphere, especially atmospheric pressure and wind stress. It is known from previous analyses that sea level fluctuations with periods of 50–70 days propagate northward along the West Coast from tropical sources (Spillane *et al.*, 1987; Enfield, 1987). It should be noted that previous analyses of subtidal fluctuations along the West Coast have typically used data adjusted for local atmospheric pressure. This is because adjusted sea level is the quantity that is most directly related to the pressure forcing of currents on the continental shelf. In the present work, we use unadjusted sea level because it is the relevant quantity for studying the effects of subtidal fluctuations on coastal hazards such as tsunamis and storm surges.

4.1 MODWT Multiresolution Analysis

Figure 1 shows the MODWT multiresolution analysis of order $J = 7$ based upon the LA(8) wavelet filter (see (15) in Appendix 3). It consists of the smooth $\widetilde{\mathcal{S}}_7$ (top of Figure 1) corresponding to variations on a scale of 64 days and greater and the seven detail series $\widetilde{\mathcal{D}}_1, \widetilde{\mathcal{D}}_2, \ldots, \widetilde{\mathcal{D}}_7$ (middle of Figure 1) associated with changes on scales of 1/2, 1, ..., 32 days, respectively. The smooth $\widetilde{\mathcal{S}}_7$ contains the annual variations in subtidal fluctuations at Crescent City (in fact our choice of $J = 7$ forces the smooth to contain these variations – going with a much larger J would break up the annual variations, while a much smaller J would add some scales to the smooth that, as we shall see, have a seasonally dependent variance). Although there is considerable variability from year to year in how $\widetilde{\mathcal{S}}_7$ varies during each year, the qualitative features of $\widetilde{\mathcal{S}}_7$ agree well with results from previous studies. For example, the highest portions of the annual variations usually occur in winter and can be attributed to low atmospheric pressure and northward winds (Chelton and Davis, 1982; Halliwell and Allen, 1984; Spillane *et al.*, 1987; Strub *et al.*, 1987b; Roden, 1989). There is also a secondary maximum during summer due to seasonal warming of the upper ocean (Pattullo *et al.*, 1955), superimposed on low summer subtidal fluctuations due to high atmospheric pressure and southward winds. The lowest portions of the annual variations at Crescent City usually happen in March or April and follow immediately after an often rapid (i.e., within a few days) spring transition in the atmosphere over the eastern North Pacific Ocean (Strub *et al.*, 1987a; Strub and James, 1988), a fact that can be verified by locating the low points on $\widetilde{\mathcal{S}}_7$ and comparing these times to records of atmospheric pressure.

The seven detail series $\widetilde{\mathcal{D}}_j$ also pick out a number of interesting features, including fluctuations that are transient in nature and limited to a few scales. As one example, Figure 2 focuses in on the 1985–6 portion of $\widetilde{\mathcal{D}}_2$, $\widetilde{\mathcal{D}}_3$ and $\widetilde{\mathcal{S}}_7$ in Figure 1 and shows that there was a brief lull in subtidal variability during December 1985 at short scales. An examination of the weather conditions during this period shows that the lull was due to the northward deflection of storms away from the Crescent City region by a high pressure ridge in the atmosphere that extended seaward from the western United States. Such ridges typically have slowly varying patterns of atmospheric pressure and winds. However, this particular ridge did not persist long enough to reverse the upward trend in seasonal water levels seen in the smooth $\widetilde{\mathcal{S}}_7$, even though both its high atmospheric pressure and light winds should tend to lower sea level at the coast. The main influence of the high pressure ridge appears to be a decrease in the variability at scales of 1 and 2 days. The tendency of having low variability at short scales when $\widetilde{\mathcal{S}}_7$ is low (and the converse of high variability when $\widetilde{\mathcal{S}}_7$ is high) can be seen throughout the multiresolution analysis in Figure 1. One reason for this behavior is the association between subtidal fluctuations and large-scale patterns in the atmosphere over the North Pacific Ocean in which the location and intensity of seasonal variations in major atmospheric features, like the Aleutian Low and the Polar Front, control the atmospheric variability at shorter scales (Palmén and Newton, 1969; Kushnir and Wallace, 1989; and Roden, 1989). Features such as the one illustrated in Figure 2 are often very difficult to spot in the original time series, but MODWT multiresolution analysis provides an investigator with tools to easily identify short scale events in subtidal fluctuations and relate them to fluctuations at longer scales and to external covariates.

The multiresolution analysis shows that particularly high events in subtidal fluctuations occur when events in details $\widetilde{\mathcal{D}}_2$ to $\widetilde{\mathcal{D}}_7$ coincide in time with high values in $\widetilde{\mathcal{S}}_7$ (note that $\widetilde{\mathcal{D}}_1$ is relatively unimportant). If these high events occur during late December or early January, there is especially high risk of coastal flooding because they then coincide with high astronomical tides around the time of the winter solstice. Conversely, persistent (longer scale) events of high atmospheric pressure and/or southward winds tend to lower sea level and suppress the occurrence of short scale events of high sea level.

4.2 MODWT Analysis of Variance

The multiresolution analysis in Figure 1 indicates that there is a seasonal dependence in the variance of the details series. For example, note that the fluctuations in $\widetilde{\mathcal{D}}_2$ tend to be larger near the beginning of each year, indicating increased variability in winter as compared to summer. As noted in Section 3.3, it is problematic to quantify the scale-dependent variance properties of $\mathbf{X}$ from a MODWT multiresolution analysis because

$$\|\mathbf{X}\|^2 \neq \sum_{j=1}^{7} \|\widetilde{\mathcal{D}}_j\|^2 + \|\widetilde{\mathcal{S}}_7\|^2.$$

To analyze the variance across time, we instead must examine the circularly shifted MODWT wavelet and scaling coefficients $\mathcal{T}^{\nu_j^{(H)}}\widetilde{\mathbf{W}}_j$ and $\mathcal{T}^{\nu_7^{(G)}}\widetilde{\mathbf{V}}_7$, for which we have the decomposition

$$\|\mathbf{X}\|^2 = \sum_{j=1}^{7} \|\mathcal{T}^{\nu_j^{(H)}}\widetilde{\mathbf{W}}_j\|^2 + \|\mathcal{T}^{\nu_7^{(G)}}\widetilde{\mathbf{V}}_7\|^2.$$

Figure 3 decomposes $\|\mathcal{T}^{\nu_j^{(H)}}\widetilde{\mathbf{W}}_j\|^2$ across time by plotting the running average of 61 squared elements of $\mathcal{T}^{\nu_j^{(H)}}\widetilde{\mathbf{W}}_j$ versus time for $j = 2, \ldots 7$ (the $j = 1$ component is relatively unimportant and is not shown henceforth). Since the sampling rate is twice per day, the running averages span approximately a month of data. The dashed horizontal lines indicate $\|\mathcal{T}^{\nu_j^{(H)}}\widetilde{\mathbf{W}}_j\|^2/N$, i.e., the contribution to the sample variance of $\mathbf{X}$ due to variations on the jth scale. The largest contributions are due to 4–16 day scales (i.e., $j = 4$, 5 and 6). This variability is associated with shifts in the weather patterns over the North Pacific Ocean occurring over the same scales. Figure 3 also shows that, while there is a clear increase in variability during most winters at scales ranging from 2 to 32 days, there are also some winters – particularly at the longer scales – for which the increase in variability is relatively small. For example, the relatively low variance at nearly every scale during the winters 1985, 1989 and 1990 can be attributed to weak storm activity in those years, in contrast to the high variance during the winters 1983 and 1987. These interannual variations in the strength of the winter variance coincide in time with El Niño/Southern Oscillation events in the Equatorial Pacific Ocean, which are known to influence seasonal sea level along the West Coast. Specifically, La Niña conditions (stronger than normal westward winds and colder than normal surface temperatures along the Equator) prevailed when the winter sea level variances were low at Crescent City; whereas El Niño conditions (occurences of eastward winds and warmer than normal surface temperatures along the Equator) prevailed when the winter variances were high.

Another look at the time and scale dependent variability is shown in Figure 4 using rotated cumulative variance plots for scales of a day (bottom plot, $j = 2$) and 32 days (top, $j = 7$), which are defined by $C_{j,t} - tC_{j,N-1}/(N-1)$, where

$$C_{j,t} \equiv \frac{1}{N}\sum_{u=0}^{t} \widetilde{W}^2_{j,u-\nu_j^{(H)} \bmod N}, \quad t = 0, \ldots, N-1.$$

These plots show what can be thought of as deviations from the expected accumulation of sample variance across time for a stationary process. The linear appearance of the bottom plot during the summer months indicates that the variability at mid-summer at a scale of a day is relatively stable and predictable from year to year. The point at which the stable summer pattern shifts into the more erratic winter pattern can change from one year to the next by up to a month; moreover, the shift appears to be fairly abrupt in some years (e.g., 1983) and diffuse in others (e.g., 1988). By contrast the top plot shows that the seasonal dependence at a scale of 32 days is much more erratic. For example, the accumulation of variance increases quite markedly around the beginning of 1980, 1982, 1983 and 1986, but is then quite constant over a 22 month span from March 1989 to January 1991.

Figure 3 suggests that a reasonable way to summarize the annual variability in the scale dependent variance is by averaging – across all 12 years – all the squared circularly shifted MODWT wavelet coefficients that fall in a given calendar month. The results of this averaging are shown in Figure 5. Under the simplifying assumptions that the wavelet coefficients over each month can be regarded as one portion of a realization of a stationary process and that the coefficients from one year to the next are independent of each other, the methodology described in Percival (1995) can be used to develop approximate 95% confidence intervals for the underlying true variances. On a logarithmic scale, the widths of these intervals are a function of scale, but do not depend on the variance estimates themselves. These widths are indicated by the vertical portions of the crisscrosses near the bottom of Figure 5. Shifting the crisscross for a particular scale so that its center falls on one of the 12 monthly variances for that scale yields an approximate 95% confidence interval. Note that the temporal patterns of variance are very similar for all 6 scales. The average variances are generally highest during the winter weather regime (November to March) and lowest in July and August, approximately 3 to 4 months after the lowest seasonal sea level of the year (cf. $\widetilde{\mathcal{S}}_7$ in Figure 1). The average winter variances are approximately 5 to 20 times the summer variances.

5. DISCUSSION

5.1 Implications for Inundation Forecasting

The MODWT analyses of subtidal sea level fluctuations have a number of important implications for the forecasting of coastal inundation near Crescent City and in other coastal regions with similar sea level characteristics. The results show that high subtidal sea level is most likely during the winter regime (November–March) due to the superposition of high seasonal and shorter scale events. The fact that the greatest sea level variance occurs at 4–16 day scales indicates that an overall sea level forecast based on the predicted tides, plus an average of subtidal sea level over the past few days, should provide a useful forecast of the sea level upon which an imminent tsunami or storm surge might occur. The average also includes deviations from the average seasonal cycle due to interannual variations, such as those caused by El Niño/Southern Oscillation events. The forecasts can be improved by taking into account the sea level response to weather that is forecast for the coastal region (of concern are shifts in the weather patterns that will change both sea level on the 4–16 day scales and the intensity of shorter scale events).

5.2 Modeling Subtidal Fluctuations

The results of Section 4 can be used to formulate a complete model for the Crescent City subtidal fluctuations $\mathbf{X}$. Such a model must account for the time-dependent features in $\mathbf{X}$ indicated by our wavelet analysis. For instance, the low variance during the summer implies that sea levels should be more predictable then than during the winter. While a full discussion of a complete model is outside the focus of the present paper, the key ideas are as follows. First, note that the regular shape of the variance curves in Figure 3 suggests an approach to modeling the annual cycle of monthly average variance in which $\log E\{\widetilde{W}_{j,t}^2\}$ is assumed to be a sum of sinusoids (e.g., with annual and semiannual terms) and a constant. Second, since the DWT coefficients $\mathbf{W}$ for $\mathbf{X}$ can be obtained by rescaling and subsampling the MODWT coefficients (see Section 3.1), we can express a model for $\mathbf{X}$ in terms of its DWT by making the simplifying assumptions that the elements of $\mathbf{W}_1, \ldots, \mathbf{W}_7$ are uncorrelated Gaussian random variables (rv's) with zero means and variances dictated by appropriately rescaling the model for $\log E\{\widetilde{W}_{j,t}^2\}$ (as discussed in Percival, 1995, the assumption of uncorrelatedness for the DWT coefficients is reasonable for broadband time series, but a similar statement does not hold for the MODWT coefficients – this is the main reason for expressing the model in terms of the DWT). Additionally, we assume that the elements of $\mathbf{V}_7$ are Gaussian rv's that are uncorrelated with both each other and the elements of $\mathbf{W}_j$ and that have a time dependent mean (estimated using standard Fourier techniques) and a constant variance.

Now suppose that $\mathbf{X}$ is partitioned into two subvectors, namely, $\mathbf{X} = [\,\mathbf{X}_p^T \quad \mathbf{X}_f^T\,]^T$, where $\mathbf{X}_p$ contains M available measured values, while $\mathbf{X}_f$ contains $N-M$ unavailable future values we want to predict. As before, let $\mathbf{W}$ be the DWT of $\mathbf{X}$, and replace all coefficients in $\mathbf{W}$ that involve elements in $\mathbf{X}_f$ by their expected values. The desired predicted values for $\mathbf{X}_f$ are obtained by taking the inverse DWT of the modified $\mathbf{W}$. An assessment of the accuracy of the predictions can be made using Monte Carlo techniques, i.e., by repetitively using random deviates generated from the assumed distributions in place of the expected values for the undetermined elements of $\mathbf{W}$.

As suggested by our analysis in Section 4, the basic model above can be refined by using atmospheric pressure as a covariate. Measured pressure values would thus be used to adjust the simple model for $\log E\{\widetilde{W}_{j,t}^2\}$ so that predicted variability is decreased when atmospheric pressure is high.

5.3 Zero Phase Filtering

As noted in Section 3.2, the details and smooths constructed by the MODWT can be regarded as outputs from zero phase filters. This zero phase property is important if we want to relate events in the details to events in the original series and if we want to understand the temporal relationships between events at different scales. To illustrate what this property of zero phase means in practice, we show in the top plot of Figure 6 portions of the MODWT detail $\widetilde{\mathcal{D}}_5$ (thin curve) and $\mathbf{X}$ (thick) around the first part of 1986. This detail should reflect changes in $\mathbf{X}$ on a scale of 8 days, so we would expect values in $\widetilde{\mathcal{D}}_5$ to be large when an average spanning about 8 days differs markedly from values surrounding it. This time period was picked because there are three peaks in $\mathbf{X}$ of such a duration – these are centered at about 32, 48 and 72 days from 1 January 1986. The MODWT detail picks out these events nicely, and the location of the peaks in $\widetilde{\mathcal{D}}_5$ roughly match those in $\mathbf{X}$. Because $\widetilde{\mathcal{D}}_5$ is invariant under circular shifts in $\mathbf{X}$, the top plot will remain the same no matter what origin we pick for $\mathbf{X}$.

By way of contrast, the thin curves in the middle and bottom plots of Figure 6 show DWT details $\mathcal{D}_5$ for two different shifts in the origin of $\mathbf{X}$, namely, 12 and 8 values (corresponding to 6 and 4 days). Note that changing the origin of $\mathbf{X}$ by 2 days changes markedly the $\mathcal{D}_5$'s. Because DWT details do not possess the zero phase property, the locations of peaks in $\mathcal{D}_5$ need not match up very well with those in $\mathbf{X}$. For example, consider the location of the peak in $\mathcal{D}_5$ corresponding to the one in $\mathbf{X}$ near 32 days. Relative to $\widetilde{\mathcal{D}}_5$ in the upper plot, the peak in $\mathcal{D}_5$ occurs markedly later in the middle plot and markedly earlier in the bottom plot. The ability of DWT details to properly locate transient events in $\mathbf{X}$ is thus limited, whereas MODWT details perform well because of their zero phase property.

5.4 Circularity Assumption

Both the DWT and the MODWT make use of circular filtering, which means that, e.g., X_{N-1} is regarded as a useful surrogate for X_{-1} for the purposes of filtering. This assumption is reasonable for some series if the sample size is chosen appropriately. For example, the subtidal fluctuations discussed in Section 4 has a strong annual component, so it can be regarded as a circular series to a good approximation because the number of samples covers about 12 complete years. We note that the circularity assumption is fairly mild here because it affects only a small number of end points for short scales. Also the additivity constraint satisfied by a MODWT multiresolution analysis ensures a certain degree of fidelity between the components of the analysis and $\mathbf{X}$.

For other series, circularity is a problematic assumption, particularly if there is a large discontinuity between X_{N-1} and X_0. Because a circularity assumption is equivalent to the periodic condition often assumed in Fourier analysis, we can make use of some of the techniques that have been successful in Fourier analysis. One simple – but effective – technique is to reflect the series at the boundaries; i.e., we append a reversed version of $\mathbf{X}$ to the end of $\mathbf{X}$ to form a circular series of length $2N$, which by construction begins and ends with X_0 (note that the reflected series has the same sample mean and variance as $\mathbf{X}$). Other possibilities for dealing with the circularity assumption include zero padding, tapering and polynomial extrapolations. A comprehensive discussion of how to handle circularity is beyond the scope of this paper, but Chapter 14 of the recent book by Bruce and Gao (1996) discusses several different options and gives practitioners guidelines for choosing a technique that is suitable for a given time series. For the Crescent City series, we found that using either a reflected series or zero padding rather than just assuming $\mathbf{X}$ to be circular made very little difference in our analysis.

5.5 Other Analysis Techniques

While we advocate the use of MODWT analysis in this paper, it is important to understand how this technique compares to others that might seem reasonable to use with time series similar to the Crescent City series. We have already indicated the key differences between MODWT and DWT analyses in Sections 3 and 5.3. Here we briefly compare MODWT analysis with two important Fourier-based techniques for handling nonstationary time series, namely, the short-time Fourier transform and complex demodulation.

While the nonstationary features of the Crescent City series that are readily picked out by MODWT analysis cannot be extracted by a traditional Fourier analysis of the entire series $\mathbf{X}$, it is possible to extract some of the same features by nonstandard use of short-time Fourier transform (STFT) analysis, which is a type of time/frequency analysis used primarily to track the evolution of narrowband signals across time (Cohen, 1995). The standard way of using STFT analysis is to choose a window size and then to conduct Fourier analyses over subsets of $\mathbf{X}$ defined by the window size. For example, if we picked a window size of 30.5 days, we could conduct a spectral analysis over each period of length 30.5 days contained in 1980 to 1991 in the Crescent City series. This STFT analysis of variance would yield a narrowband decomposition of $\mathbf{X}$ across each 30.5 day period, and the results would usually be displayed as a color-coded plot showing variations in $\mathbf{X}$ at particular frequencies and centered at particular times. Since the MODWT coefficients $\widetilde{W}_{j,t}$ reflect variations over the broadband interval from $1/2^j$ to $1/2^{j-1}$ cycles per day, we could use the 30.5 day STFT to extract monthly variations analogous to those in Figure 5 at scales of 1, 2 and 4 days ($j = 1$, 2 and 3, respectively) by averaging the STFT spectral analyses across appropriate frequency bands;

by increasing the window size, the same could be done for 8, 16 and 32 days. This nonstandard application of STFT spectral analysis (i.e., averaging across frequencies and piecing together averages from different window sizes) would closely mimic MODWT analysis. Reasons for preferring MODWT analysis over standard STFT analysis for the Crescent City series are the following. First, the Crescent City series does not have time-varying narrowband features, so a few MODWT coefficients can succinctly summarize what a large number of STFT coefficients would tell us about the time-varying broadband properties of the data. Second, MODWT coefficients are computed via a scheme whereby the time series $\mathbf{X}$ is automatically looked at through a variety of window sizes commensurate with scales $\tau_j \Delta t$, whereas STFT coefficients are computed using a user-selected window size. Because the Crescent City series has time-varying features over a variety of scales (e.g., short scale transients and seasonally dependent variability), we would need to conduct STFT analyses with a variety of windows, and there is no natural way of tying these different analyses together to, e.g., formulate a model similar to the wavelet-based one described in Section 5.2.

Complex demodulation (CD) is a technique for analyzing nonstationary time series in which the series is multiplied by a series defined by the complex exponential $e^{i2\pi f t \Delta t}$ and then filtered using a narrowband low-pass filter to obtain a complex-valued series that reflects the variations in the series over a small band of frequencies centered about f (Bloomfield, 1976). As is true for STFT analysis, we could use a nonstandard version of CD to pick out variations analogous to those shown in Figure 5 for MODWT analysis. This nonstandard CW would use a set of frequencies centered about intervals from $1/2^j$ to $1/2^{j-1}$ cycles per day and would make the width of the passband equal to $1/2^j$ cycles per day. Reasons for preferring MODWT analysis over standard CD for the Crescent City series are quite similar for not preferring STFT analysis, namely, that CD is usually thought of as a narrowband technique intended to examine variations around single frequencies, whereas the series under study exhibits broadband variations; furthermore, there is no natural way to tie together CDs for different frequencies to come up with a model analogous to the one in Section 5.2.

6. CONCLUSIONS

Wavelet analysis seems ideally suited for describing subtidal sea level and other geophysical series with nonstationary or transient components. The analysis given in this paper illustrates how the maximal overlap discrete wavelet transform (MODWT) provides a succinct way of quantifying the nonstationary characteristics of time series. Similar results could be obtained by applying a set of short-time Fourier transforms to the time series if these transforms are utilized in a nonstandard way. However, wavelet methods are more straight-forward to apply and guarantee additivity for both the multiresolution and variance analyses. The MODWT offers some advantages over the orthonormal DWT. The results of the MODWT are insensitive to circular shifts of the series and to the series length. Further, the details and smooths from the MODWT multiresolution analyses can be interpreted as linear filter outputs in which events in the details and smooths have proper alignment with respect to events in the original series, an essential property when relating events across scales. Series of rotated cumulative variance show clearly the temporal variations of variance across scales. By applying known shifts to the MODWT variance series, the events in variance are also aligned relative to the time series. The pseudo-code in the appendix should make it easy for data analysts to apply the MODWT to other data sets.

The MODWT analysis of subtidal sea level fluctuations at Crescent City shows that these fluctuations are strongest during the winter regime (November–March) and occur preferentially at the scales 4–16 days. The occurrence of storm-related fluctuations tends to be modulated by longer scales associated with weather patterns that steer storms to – or away from – the Crescent City region. There are interannual variations in both the seasonal and intraseasonal fluctuations that coincide with major El Niño/Southern Oscillation events in the Equatorial Pacific Ocean. When superimposed on high astronomical tides, the subtidal fluctuations can contribute to coastal inundation by tsunamis, storm surges and high waves. However, the well-defined annual cycle of the variance indicates that a statistical model of the fluctuations can be developed that would be useful for planning purposes. The persistence implied by the 4–16 day scales suggests that short-term forecasts can be generated that would be useful during tsunami and storm surge emergencies, especially if sea level forecasts are augmented by response models of the coastal sea level to forecasted weather forcing. While not discussed explicitly in this paper, low sea level events are also of interest because they are hazards to navigation and have important implications for coastal ecosystems. The

MODWT analysis provides a basis for characterizing these events as well.

ACKNOWLEDGMENTS

The authors wish to thank Ned Cokelet, Bill Hess, Emma McCoy and Andrew Walden for helpful comments that improved this paper considerably. This research was funded in part by the NOAA Coastal Ocean Program (Contribution No. 1626 of the Pacific Marine Environmental Laboratory, NOAA, and Contribution No. 279 of the Joint Institute for the Study of the Atmosphere and Ocean, University of Washington).

APPENDIX 1: PSEUDO-CODE FOR MODWT

Here we give pseudo-code that can be used to compute the MODWT and its inverse. Let $\widetilde{V}_{0,t} \equiv X_t$ for $t = 0, \ldots, N-1$, where N is any positive integer. Let $\{\tilde{h}_n \equiv \tilde{h}_{1,n} \equiv h_{1,n}/\sqrt{2} : n = 0, \ldots, L_1 - 1\}$ be a rescaled wavelet filter of even length L_1 (see, e.g., Equation (15) in Appendix 3). Let $\{\tilde{g}_n \equiv \tilde{g}_{1,n} \equiv g_{1,n}/\sqrt{2}\}$ be the corresponding rescaled scaling filter (cf. Equation (2)). Denote the elements of $\widetilde{\mathbf{W}}_j$ and $\widetilde{\mathbf{V}}_J$ as $\widetilde{W}_{j,t}$ and $\widetilde{V}_{J,t}$, $t = 0, \ldots, N-1$. Given $\widetilde{\mathbf{V}}_{j-1}$, the following pseudo-code computes $\widetilde{\mathbf{W}}_j$ and $\widetilde{\mathbf{V}}_j$:

For $t = 0, \ldots, N-1$, do the outer loop:
  Set k to t.
  Set $\widetilde{W}_{j,t}$ to $\tilde{h}_0 \widetilde{V}_{j-1,k}$, and set $\widetilde{V}_{j,t}$ to $\tilde{g}_0 \widetilde{V}_{j-1,k}$.
  For $n = 1, \ldots, L_1 - 1$, do the inner loop:
    Decrement k by 2^{j-1}.
    If $k < 0$, set k to $k \mod N$.
    Increment $\widetilde{W}_{j,t}$ by $\tilde{h}_n \widetilde{V}_{j-1,k}$, and increment $\widetilde{V}_{j,t}$ by $\tilde{g}_n \widetilde{V}_{j-1,k}$.
  End of inner loop.
End of outer loop.

Note that, if j is such that $2^{j-1} \leq N$ (as will usually be the case in practical applications), then the single '$k \mod N$' in the above code can be replaced by '$k + N$.' By using the pseudo-code above first for $j = 1$ (i.e., starting with $\widetilde{\mathbf{V}}_0 = \mathbf{X}$) and then successively for $j = 2, \ldots, J$, we obtain the component vectors of the MODWT, namely, $\widetilde{\mathbf{W}}_1, \ldots, \widetilde{\mathbf{W}}_J$ and $\widetilde{\mathbf{V}}_J$, along with the intermediate vectors $\widetilde{\mathbf{V}}_1, \ldots \widetilde{\mathbf{V}}_{J-1}$.

The task of the inverse MODWT is to compute $\mathbf{X}$ given the MODWT vectors $\widetilde{\mathbf{W}}_1, \ldots, \widetilde{\mathbf{W}}_J$ and $\widetilde{\mathbf{V}}_J$. Given $\widetilde{\mathbf{W}}_j$ and $\widetilde{\mathbf{V}}_j$, the following pseudo-code computes $\widetilde{\mathbf{V}}_{j-1}$:

For $t = 0, \ldots, N-1$, do the outer loop:
  Set k to t.
  Set $\widetilde{V}_{j-1,t}$ to $\tilde{h}_0 \widetilde{W}_{j,k} + \tilde{g}_0 \widetilde{V}_{j,k}$.
  For $n = 1, \ldots, L_1 - 1$, do the inner loop:
    Increment k by 2^{j-1}.
    If $k \geq N$, set k to $k \mod N$.
    Increment $\widetilde{V}_{j-1,t}$ by $\tilde{h}_n \widetilde{W}_{j,k} + \tilde{g}_n \widetilde{V}_{j,k}$.
  End of the inner loop.
End of the outer loop.

Note that, if j is such that $2^{j-1} \leq N$, then the single '$k \mod N$' in the above code can be replaced by '$k - N$.' By using the pseudo-code above first for $j = J$ (i.e., starting with $\widetilde{\mathbf{W}}_J$ and $\widetilde{\mathbf{V}}_J$) and then successively for $j = J-1, \ldots, 1$, we obtain $\widetilde{\mathbf{V}}_{J-1}, \ldots, \widetilde{\mathbf{V}}_1$ and finally $\widetilde{\mathbf{V}}_0 = \mathbf{X}$.

The jth detail $\widetilde{\mathcal{D}}_j$ can be obtained by taking the inverse MODWT of the $j+1$ vectors $\widetilde{\mathbf{0}}_1, \ldots, \widetilde{\mathbf{0}}_{j-1}$, $\widetilde{\mathbf{W}}_j$ and $\widetilde{\mathbf{0}}_j$, where $\widetilde{\mathbf{0}}_k$, $k = 1, \ldots, j$, is a vector of N zeros. This detail can be computed by iterating the inverse MODWT algorithm over $j, j-1, \ldots, 1$ starting with $\widetilde{\mathbf{W}}_j$ and with $\widetilde{\mathbf{0}}_j$ substituted for $\widetilde{\mathbf{V}}_j$ in the above pseudo-code. At the end of j iterations, the desired $\widetilde{\mathcal{D}}_j$ will be stored in $\widetilde{\mathbf{V}}_0$. Likewise, the smooth $\widetilde{\mathcal{S}}_J$ can be obtaining by applying the inverse DWT to the $J+1$ vectors $\widetilde{\mathbf{0}}_1, \ldots, \widetilde{\mathbf{0}}_J$ and $\widetilde{\mathbf{V}}_J$.

APPENDIX 2: PROOFS OF BASIC MODWT PROPERTIES

Proof of Equation (9):

Since the tth elements of $\widetilde{\mathcal{D}}_j$ and $\widetilde{\mathcal{S}}_J$ are by definition $\widetilde{\mathbf{W}}_j^T \mathcal{T}^t \tilde{\mathbf{h}}_j^*$ and $\widetilde{\mathbf{V}}_J^T \mathcal{T}^t \tilde{\mathbf{g}}_J^*$, we need to show that

$$X_t = \sum_{j=1}^{J} \widetilde{\mathbf{W}}_j^T \mathcal{T}^t \tilde{\mathbf{h}}_j^* + \widetilde{\mathbf{V}}_J^T \mathcal{T}^t \tilde{\mathbf{g}}_J^*, \quad t = 0, \ldots, N-1.$$

If we let $\mathcal{X}_k$ denote the DFT of the X_t's, the above is equivalent to showing that

$$\mathcal{X}_k = \sum_{j=1}^{J} \sum_{t=0}^{N-1} \widetilde{\mathbf{W}}_j^T \mathcal{T}^t \tilde{\mathbf{h}}_j^* e^{-i2\pi tk/N} + \sum_{t=0}^{N-1} \widetilde{\mathbf{V}}_J^T \mathcal{T}^t \tilde{\mathbf{g}}_J^* e^{-i2\pi tk/N}, \quad k = 0, \ldots, N-1. \tag{11}$$

Since the sequence $\widetilde{\mathbf{W}}_j^T \mathcal{T}^t \tilde{\mathbf{h}}_j^*$ is a circular convolution of $\widetilde{\mathbf{W}}_j$ with the filter $\tilde{\mathbf{h}}_j^*$, its DFT is given by the product of the DFTs for $\widetilde{\mathbf{W}}_j$ and $\tilde{\mathbf{h}}_j^*$. As indicated in Section 3.2, the DFT of $\tilde{\mathbf{h}}_j^*$ is given by $H_{j,k}^*/2^{j/2}$, i.e., the complex conjugate of $H_{j,k}/2^{j/2}$. Since the elements of $\widetilde{\mathbf{W}}_j$ are obtained by circularly convolving $\mathbf{X}$ with the filter $\tilde{\mathbf{h}}_j = \mathbf{h}_j/2^{j/2}$, the DFT of $\widetilde{\mathbf{W}}_j$ is equal to the product of the DFTs for $\mathbf{X}$ and $\tilde{\mathbf{h}}_j$, namely, $\mathcal{X}_k H_{j,k}/2^{j/2}$. Using an analogous argument for the DFT of $\widetilde{\mathbf{V}}_J^T \mathcal{T}^t \tilde{\mathbf{g}}_J^*$, the right-hand side of (11) is equal to

$$\sum_{j=1}^{J} \frac{1}{2^j} \mathcal{X}_k H_{j,k} H_{j,k}^* + \frac{1}{2^J} \mathcal{X}_k G_{J,k} G_{J,k}^* = \mathcal{X}_k \left(\sum_{j=1}^{J} \frac{1}{2^j} \left| H_{j,k} \right|^2 + \frac{1}{2^J} \left| G_{J,k} \right|^2 \right),$$

so the desired result follows if we can show that

$$\sum_{j=1}^{J} \frac{1}{2^j} \left| H_{j,k} \right|^2 + \frac{1}{2^J} \left| G_{J,k} \right|^2 = 1. \tag{12}$$

To see that (12) holds for $J = 1$, note that Equation (1) implies that

$$\left| H_{1,k} \right|^2 + \left| G_{1,k} \right|^2 = 2 \tag{13}$$

for all k (see Equations (5.1.20) and (5.1.39) of Daubechies, 1992). Assume now that (12) holds when J is replaced by $J-1$. To see that this implies that (12) holds for J, use the definitions for $H_{j,k}$ and $G_{J,k}$ given in Equations (3) and (4) to obtain

$$\begin{aligned}
&\sum_{j=1}^{J} \frac{1}{2^j} \left| H_{j,k} \right|^2 + \frac{1}{2^J} \left| G_{J,k} \right|^2 \\
&= \sum_{j=1}^{J-1} \frac{1}{2^j} \left| H_{j,k} \right|^2 + \frac{1}{2^J} \left(\left| H_{1,2^{J-1}k \bmod N} \right|^2 + \left| G_{1,2^{J-1}k \bmod N} \right|^2 \right) \prod_{l=0}^{J-2} \left| G_{1,2^l k \bmod N} \right|^2 \\
&= \sum_{j=1}^{J-1} \frac{1}{2^j} \left| H_{j,k} \right|^2 + \frac{1}{2^{J-1}} \left| G_{J-1,k} \right|^2 = 1,
\end{aligned}$$

which establishes the desired result.

Proof of Equation (10):

With $\widetilde{\mathbf{V}}_0 \equiv \mathbf{X}$, Equation (10) follows readily if we can establish that

$$\|\widetilde{\mathbf{V}}_{j-1}\|^2 = \|\widetilde{\mathbf{W}}_j\|^2 + \|\widetilde{\mathbf{V}}_j\|^2, \qquad j = 1, \ldots, J. \tag{14}$$

Since N times the norm of a vector is equal to the norm of its DFT (Parseval's theorem); since $\widetilde{\mathbf{W}}_j$ is the circular convolution of $\mathbf{X}$ and $\tilde{\mathbf{h}}_j$; since the DFT of a convolution is the product of the DFTs of its components; and since the DFTs of $\mathbf{X}$ and $\tilde{\mathbf{h}}_j$ are given by $\mathcal{X}_k$ and $H_{j,k}/2^{j/2}$, we have

$$\|\widetilde{\mathbf{W}}_j\|^2 = \frac{1}{2^j N}\sum_{k=0}^{N-1} |\mathcal{X}_k|^2\,|H_{j,k}|^2\,;\ \text{likewise,}\quad \|\widetilde{\mathbf{V}}_j\|^2 = \frac{1}{2^j N}\sum_{k=0}^{N-1} |\mathcal{X}_k|^2\,|G_{j,k}|^2\,.$$

Equation (14) thus follows if we can show that $2\,|G_{j-1,k}|^2 = |H_{j,k}|^2 + |G_{j,k}|^2$ (we define $G_{0,k} = 1$). Using Equations (3), (4) and (13), we have

$$|H_{j,k}|^2 + |G_{j,k}|^2 = \left(\left|H_{1,2^{j-1}k \bmod N}\right|^2 + \left|G_{1,2^{j-1}k \bmod N}\right|^2\right)|G_{j-1,k}|^2 = 2\,|G_{j-1,k}|^2\,,$$

which establishes Equation (10).

APPENDIX 3: SHIFTS FOR WAVELET AND SCALING FILTERS

Daubechies (1992) developed the class of "least asymmetric" (LA) wavelets to approximate linear phase filters as closely as possible. For example, the rescaled LA(8) wavelet filter consists of the following 8 coefficients:

$$\begin{array}{ll} \tilde{h}_{1,0} = 0.022785172948 & \tilde{h}_{1,4} = 0.568329121704 \\ \tilde{h}_{1,1} = 0.008912350721 & \tilde{h}_{1,5} = -0.351869534328 \\ \tilde{h}_{1,2} = -0.070158812089 & \tilde{h}_{1,6} = -0.020955482562 \\ \tilde{h}_{1,3} = -0.210617267102 & \tilde{h}_{1,7} = 0.053574450709 \end{array} \qquad (15)$$

The source of these coefficients is the "$N = 4$" entry of Table 6.3, p. 198, Daubechies (1992). The coefficients in that table were divided by 2 to yield the rescaled LA(8) scaling filter $\tilde{g}_{1,n}$ with normalization $\sum \tilde{g}_{1,n}^2 = 1/2$ – the above $\tilde{h}_{1,n}$'s were obtained via the relationship $\tilde{h}_{1,n} = (-1)^n \tilde{g}_{1,L_1-1-n}$ (cf. Equation (2)). The same table also gives coefficients for filters of lengths 10, 12, ..., 20. McCoy *et al.* (1995) establish that $\tilde{h}_{1,n}$ and $\tilde{g}_{1,n}$ and the higher order filters $\tilde{h}_{j,n}$ and $\tilde{g}_{j,n}$ can be converted to approximate zero phase filters if the filter outputs are (circularly) shifted by appropriate amounts, namely,

$$\nu_j^{(H)} \equiv \begin{cases} -\frac{L_j}{2}, & \text{if } L_1/2 \text{ is even;} \\ -\frac{L_j}{2}+1, & \text{if } L_1 = 10 \text{ or } 18; \\ -\frac{L_j}{2}-1, & \text{if } L_1 = 14, \end{cases}$$

for the wavelet filters and

$$\nu_j^{(G)} \equiv \begin{cases} -\frac{(L_j-1)(L_1-2)}{2(L_1-1)}, & \text{if } L_1/2 \text{ is even;} \\ -\frac{(L_j-1)L_1}{2(L_1-1)}, & \text{if } L_1 = 10 \text{ or } 18; \\ -\frac{(L_j-1)(L_1-4)}{2(L_1-1)}, & \text{if } L_1 = 14, \end{cases}$$

for the scaling filters (in the above $L_j \equiv (2^j-1)(L_1-1)+1$ is the number of nonzero coefficients in $\tilde{h}_{j,n}$). The above shifts hold only if the LA(10), LA(14), and LA(18) scaling coefficients are taken in reverse order from their tabulation in Daubechies (1992).

REFERENCES

Barnes, J. A., Chi, A. R., Cutler, L. S., Healey, D. J., Leeson, D. B., McGunigal, T. E., Mullen, J. A., Jr., Smith, W. L., Sydnor, R. L., Vessot, R. F. C. and Winkler, G. M. R. (1971), "Characterization of Frequency Stability," *IEEE Transactions on Instrumentation and Measurement*, 20, 105–120.

Bloomfield, P. (1976), *Fourier Analysis of Time Series: An Introduction*, New York: John Wiley & Sons.

Bruce, A., and Gao, H.-Y. (1996), *Applied Wavelet Analysis with S-PLUS*, New York: Springer.

Chelton, D. B., and Davis, R. E. (1982), "Monthly Mean Sea-Level Variability along the West Coast of North America," *Journal of Physical Oceanography*, 12, 757–784.

Cohen, L. (1995), *Time-Frequency Analysis*, Englewood Cliffs, N. J.: Prentice Hall.

Coifman, R. R., and Donoho, D. (1995), "Translation-Invariant De-Noising," in *Wavelets and Statistics* (Lecture Notes in Statistics, vol. 103), eds. A. Antoniadis and G. Oppenheim, New York: Springer–Verlag, 125–150.

Daubechies, I. (1992), *Ten Lectures on Wavelets*, Philadelphia: SIAM.

Denbo, D. W., and Allen, J. S. (1987), "Atmospheric Forcing of Shelf Currents and Coastal Sea Level off the West Coast of North America: May–July, 1981 and 1982," *Journal of Geophysical Research*, 92, 1,757–1,782.

Enfield, D. B. (1987), "The Intraseasonal Oscillation in Eastern Pacific Sea Levels: How is it Forced?," *Journal of Physical Oceanography*, 17, 1860–1876.

Greenhall, C. A. (1991), "Recipes for Degrees of Freedom of Frequency Stability Estimators," *IEEE Transactions on Instrumentation and Measurements*, 40, 994–999.

Halliwell, G. R., Jr., and Allen, J. S. (1984), "Atmospheric Forcing along the West Coast of North America, Summer 1973," *Journal of Physical Oceanography*, 14, 864–886.

Hamming, R. W. (1989), *Digital Filters* (Third Edition), Englewood Cliffs, N. J.: Prentice Hall.

Hickey, B. M. (1989), "Patterns and Processes of Circulation over the Washington Continental Shelf and Slope," in *Coastal Oceanography of Washington and Oregon*, eds. M. R. Landry and B. M. Hickey, Amsterdam: Elsevier Oceanography Series, 47, 41–115.

Lander, J. F., and Lockridge, P.A. (1989), *United States Tsunamis (Including United States Possessions) 1690–1988*, Boulder, CO: NOAA NGDC Publication 41–42.

Lindsay, R. W., Percival, D. B., and Rothrock, D. A. (1996), "The Discrete Wavelet Transform and the Scale Analysis of the Surface Properties of Sea Ice," *IEEE Transactions on Geoscience and Remote Sensing*, 34, 771–787.

Liang, J., and Parks, T. W. (1996), "A Translation-Invariant Wavelet Representation Algorithm with Applications," *IEEE Transactions on Signal Processing*, 44, 225–232.

Mallat, S. G. (1989), "A Theory for Multiresolution Signal Decomposition: The Wavelet Representation," *IEEE Transactions on Pattern Analysis and Machine Intelligence*, 11, 674–693.

McCoy, E. J., Percival, D. B., and Walden, A. T. (1995), "On The Phase of Least-Asymmetric Scaling and Wavelet Filters," Technical Report TR–95–15, Statistics Section, Imperial College, London.

McCoy, E. J., and Walden, A. T. (1996), "Wavelet Analysis and Synthesis of Stationary Long-Memory Processes," *Journal of Computational and Graphical Statistics*, 5, 26–56.

Meyer, Y. (1993), *Wavelets: Algorithms and Applications*, Philadelphia: SIAM.

Mofjeld, H. O., González, F. I., and Newman, J. C. (1997a), "Short-Term Forecasts of Inundation during Teletsunamis in the Eastern North Pacific Ocean," in *Perspectives on Tsunami Hazard Reduction*, ed. J. Hebenstreit, Dordrecht, NL: Kluwer, in press.

Mofjeld, H. O., González, F. I., and Newman, J. C. (1997b), "Tsunami Prediction in U.S. Coastal Regions," in *Coastal Ocean Prediction*, ed. C. Mooers, Washington D.C.: American Geophysical Union, submitted.

Nason, G. P., and Silverman, B. W. (1994), "The Discrete Wavelet Transform in S," *Journal of Computational and Graphical Statistics*, 3, 163–191.

Nason, G. P., and Silverman, B. W. (1995), "The Stationary Wavelet Transform and Some Statistical Applications," in *Wavelets and Statistics* (Lecture Notes in Statistics, vol. 103), eds. A. Antoniadis and G. Oppenheim, New York: Springer–Verlag, 281–299.

Newland, D. E. (1993), *An Introduction to Random Vibrations, Spectral & Wavelet Analysis*, New York: Longman Scientific & Technical.

Pattullo, J., Munk, W., Revelle, R., and Strong, E. (1955), "The Seasonal Oscillation in Sea Level," *Journal of Marine Research*, 14, 88–155.

Percival, D. B. (1995), "On Estimation of the Wavelet Variance," *Biometrika*, 82, 619–631.

Percival, D. B., and Guttorp, P. (1994), "Long-Memory Processes, the Allan Variance and Wavelets," in *Wavelets in Geophysics*, eds. E. Foufoula–Georgiou and P. Kumar, San Diego: Academic Press, 325–344.

Pesquet, J.-C., Krim, H., and Carfantan, H. (1996), "Time-Invariant Orthonormal Wavelet Representations," *IEEE Transactions on Signal Processing*, 44, 1964–1970.

Petrauskas, C., and Borgman, L. E. (1971), "Frequencies of Crest Heights for Random Combinations of

Astronomical Tides and Tsuanmis Recorded at Crescent City, California," Technical Report 16–8, Hydraulics Engineering Laboratory, University of California, Berkeley.
Press, W. H., Teukolsky, S. A., Vetterling, W. T., and Flannery, B. P. (1992), *Numerical Recipes: The Art of Scientific Computing* (Second Edition), Cambridge, UK: Cambridge University Press.
Pugh, D. T. (1987), *Tides, Surges and Mean Sea-Level*, New York: John Wiley.
Roden, G. I. (1960), "On the Nonseasonal Variations in Sea Level along the West Coast of North America," *Journal of Geophysical Research*, 65, 2,800–2,826.
Roden, G. I. (1989), "Analysis and Interpretation of Long-Term Climatic Variability along the West Coast of North America," in *Aspects of Climate Variability in the Pacific and the Western Americas*, ed. D. H. Peterson, Geophysical Monograph 55, Washington, D. C.: American Geophysical Union, 93–111.
Shensa, M. J. (1992), "The Discrete Wavelet Transform: Wedding the À Trous and Mallat Algorithms," *IEEE Transactions on Signal Processing*, 40, 2464–2482.
Spillane, M. C., Enfield, D. B., and Allen, J. S. (1987), "Intraseasonal Oscillations in Sea Level along the West Coast of the Americas," *Journal of Physical Oceanography*, 17, 313–325.
Strang, G. (1993), "Wavelet Transforms Versus Fourier Transforms," *Bulletin of the American Mathematical Society*, 28, 288–305.
Strub, P. T., Allen, J. S., Huyer, A., and Smith, R .L. (1987a), "Large-Scale Structure of the Spring Transition in the Coastal Ocean off Western North America," *Journal of Geophysical Research*, 92, 1,527–1,544.
Strub, P. T., Allen, J. S., Huyer, A., Smith, R .L., and Beardsley, R. C. (1987b), "Seasonal Cycles of Currents, Temperatures, Winds, and Sea Level Over the Northeast Pacific Continental Shelf: 35 N to 48 N," *Journal of Geophysical Research*, 92, 1,507–1,526.
Strub, P. T., and James, C. (1988), "Atmospheric Conditions during the Spring and Fall Transitions in the Coastal Ocean off the Western United States," *Journal of Geophysical Research*, 93, 15,561–15,584.

FIGURE CAPTIONS

Figure 1. MODWT multiresolution analysis of Crescent City subtidal sea level fluctuations based upon the LA(8) wavelet filter. The fluctuations $\mathbf{X}$ are plotted at the bottom (the mark above each labeled year indicates the beginning of that year), while the eight time series above $\mathbf{X}$ show, from the bottom on up, the details $\widetilde{\mathcal{D}}_1, \ldots, \widetilde{\mathcal{D}}_7$ and the smooth $\widetilde{\mathcal{S}}_7$. The detail $\widetilde{\mathcal{D}}_j$ is associated with changes on a scale of $\tau_j \Delta t = 2^{j-2}$ days, while the smooth $\widetilde{\mathcal{S}}_7$ is associated with variations on scales of 64 days and higher. (As of 1997, the 8746 values comprising $\mathbf{X}$ could be obtained via electronic mail by sending a message with the single line "`send percival-m from jasadata`" to the Internet address `statlib@lib.stat.cmu.edu`, which is the address for StatLib, a statistical archive maintained by Carnegie–Mellon University. The data are also accessible via the StatLib Web site at `http://lib.stat.cmu.edu/`.)

Figure 2. Portion of multiresolution analysis for Crescent City series showing details $\widetilde{\mathcal{D}}_2$ (1 day scale) and $\widetilde{\mathcal{D}}_3$ (2 day scale) and smooth $\widetilde{\mathcal{S}}_7$ for years 1985–86.

Figure 3. MODWT analysis of variance of Crescent City series. The six plotted series are running 61 point (30.5 day) averages of the squared circularly shifted MODWT wavelet coefficients $\widetilde{W}_{j,t}$ for $j = 2$ (scale of 1 day; bottom of plot) to $j = 7$ (scale of 32 days; top of plot). The dashed horizontal lines indicated the squared $\widetilde{W}_{j,t}$'s averaged over all t.

Figure 4. Rotated cumulative variance plots for circularly shifted MODWT wavelet coefficients $\widetilde{W}_{2,t}$ (scale of 1 day; bottom plot) and $\widetilde{W}_{7,t}$ (scale of 32 days; top plot).

Figure 5. Averages of squared circularly shifted MODWT wavelet coefficients $\widetilde{W}_{j,t}$ grouped by months across 12 years (1980–91). The six curves show the averaged squared coefficients for scales $j = 2$ (scale of 1 day) to $j = 7$ (scale of 32 days). The height of one of the six crisscrosses at the bottom of the plot indicates the width (on a logarithmic scale) of a 95% confidence interval for a point on the curve for the corresponding scale.

Figure 6. Demonstration of zero phase property of MODWT details. The thick curve in each of the three plots is the Crescent City series for a period encompassing the first quarter of 1986. The thin curve in the top plot shows the MODWT detail $\widetilde{\mathcal{D}}_5$ (scale of 8 days), while the corresponding curves in the other two plots show the DWT detail $\mathcal{D}_5$ under two choices for the beginning of the entire Crescent City series $\mathbf{X}$ (the first choice displaces the origin of $\mathbf{X}$ by 12 data values (6 days), and the second, by 8 values (4 days)).

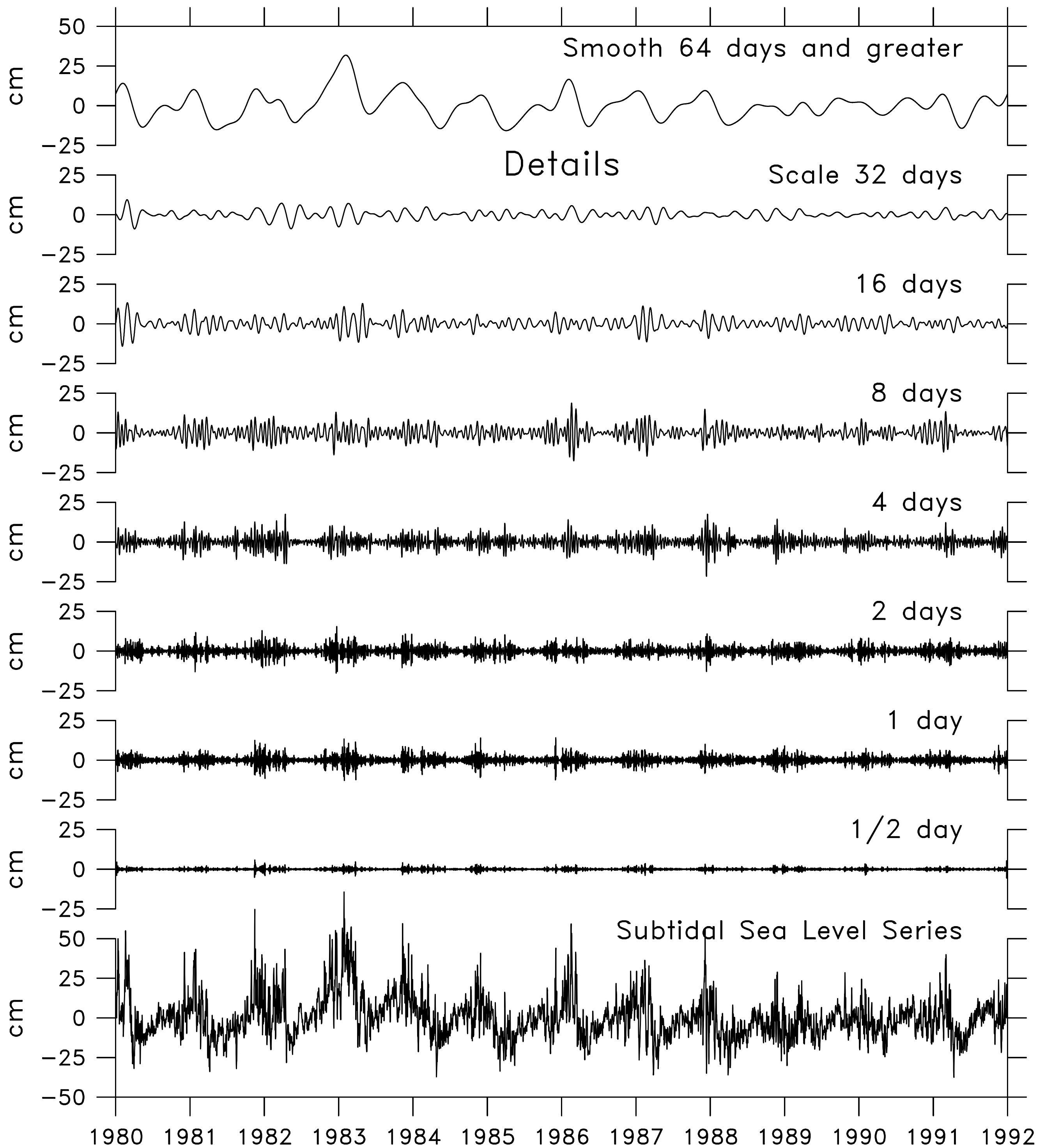

Smooth 64 days and greater
Details
Scale 32 days
16 days
8 days
4 days
2 days
1 day
1/2 day
Subtidal Sea Level Series
cm
50
25
0
−25
−50
1980
1981
1982
1983
1984
1985
1986
1987
1988
1989
1990
1991
1992

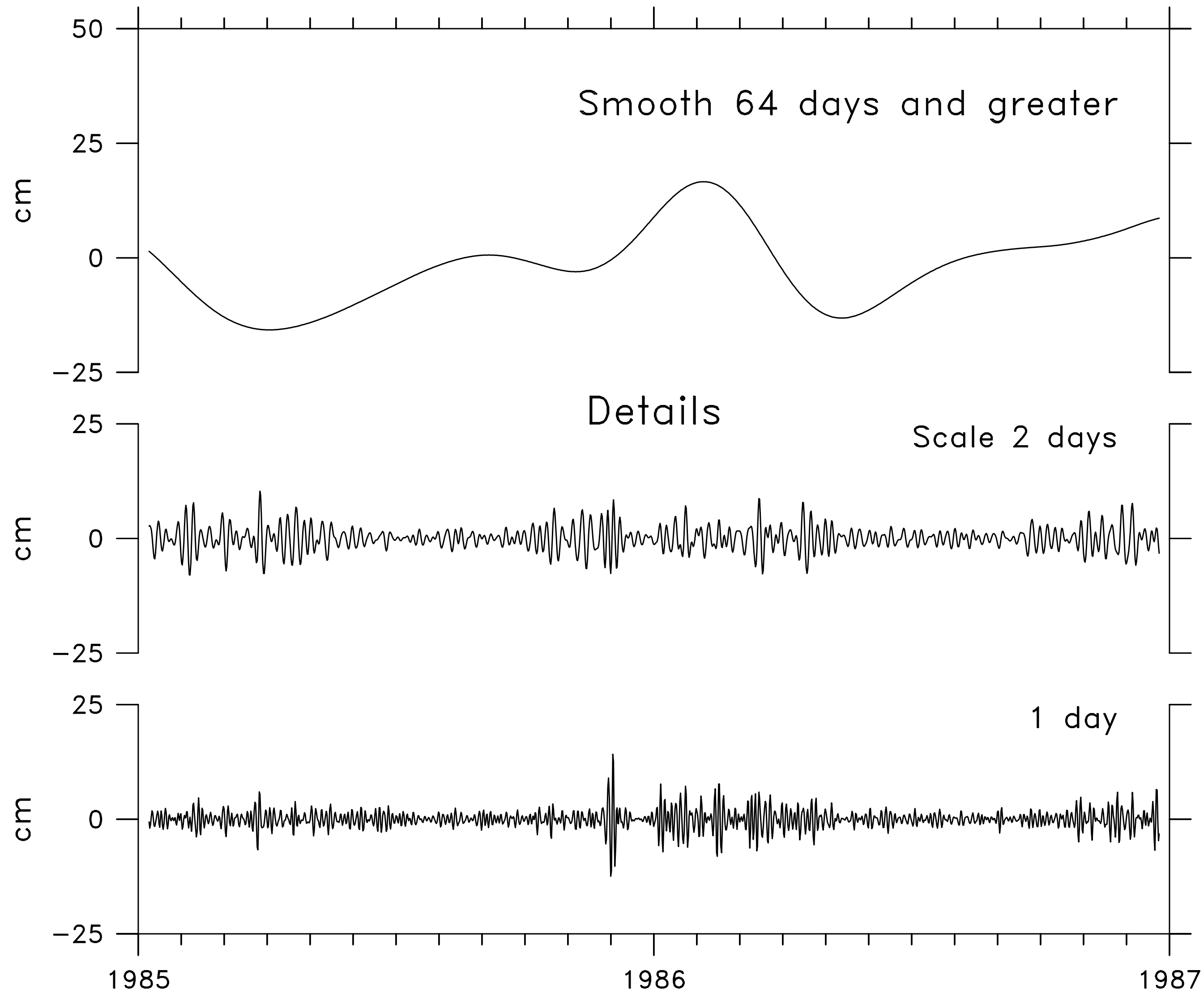

Smooth 64 days and greater
Details
Scale 2 days
1 day
cm
50
25
0
−25
1985
1986
1987

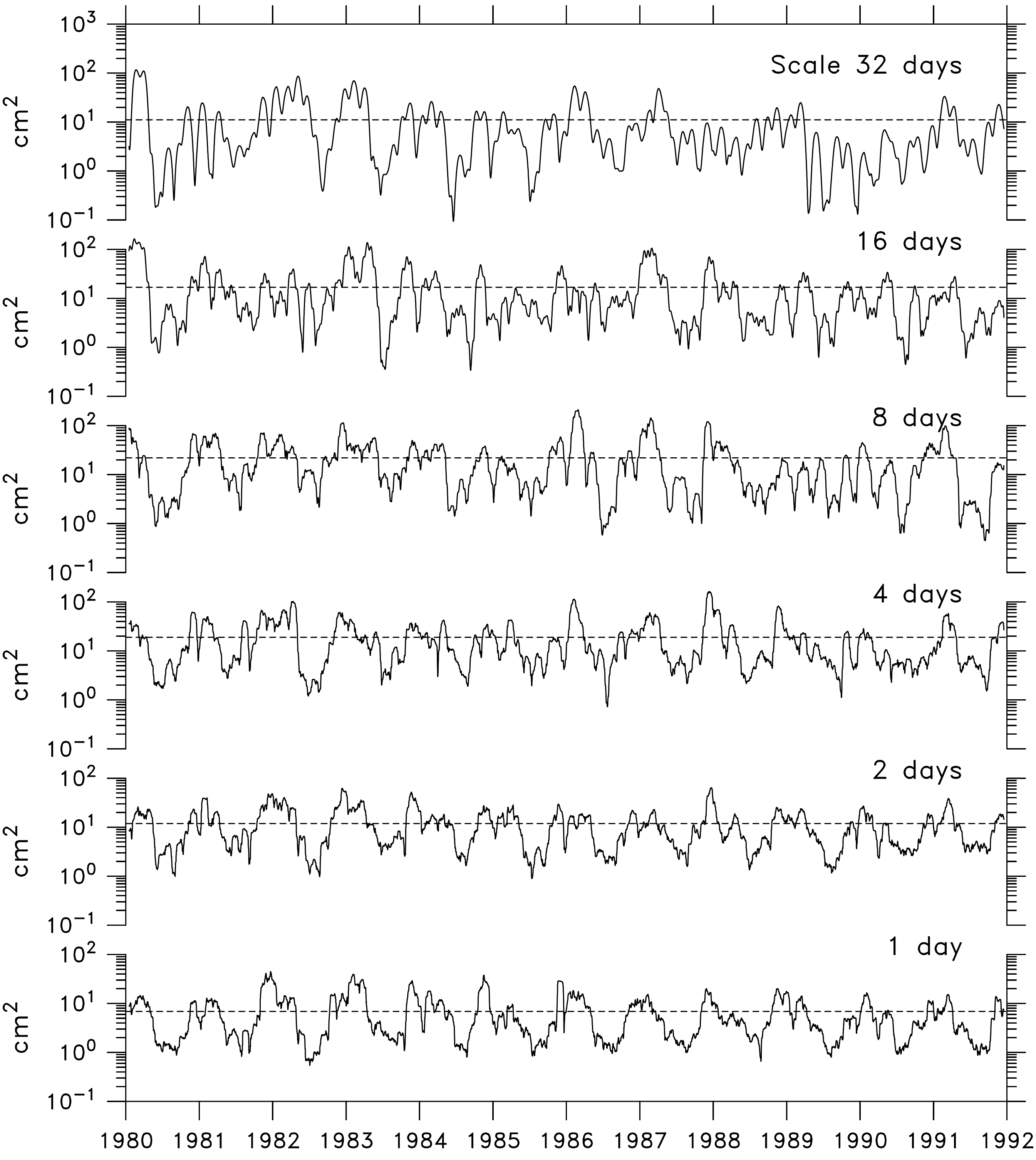
Scale 32 days
16 days
8 days
4 days
2 days
1 day
cm^2
10^{-1}
10^0
10^1
10^2
10^3
1980
1981
1982
1983
1984
1985
1986
1987
1988
1989
1990
1991
1992

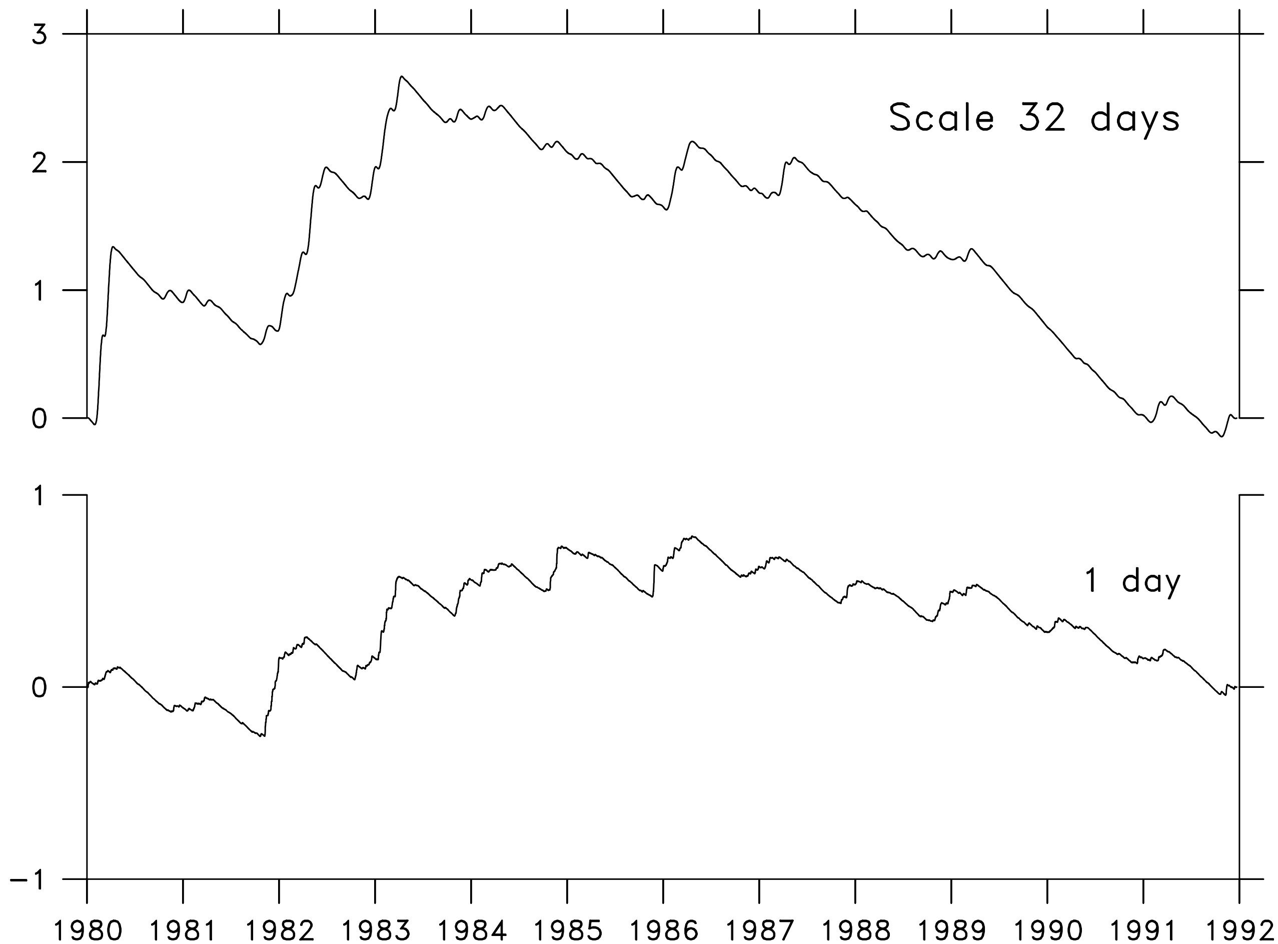
Scale 32 days
1 day
3
2
1
0
1
0
−1
1980
1981
1982
1983
1984
1985
1986
1987
1988
1989
1990
1991
1992

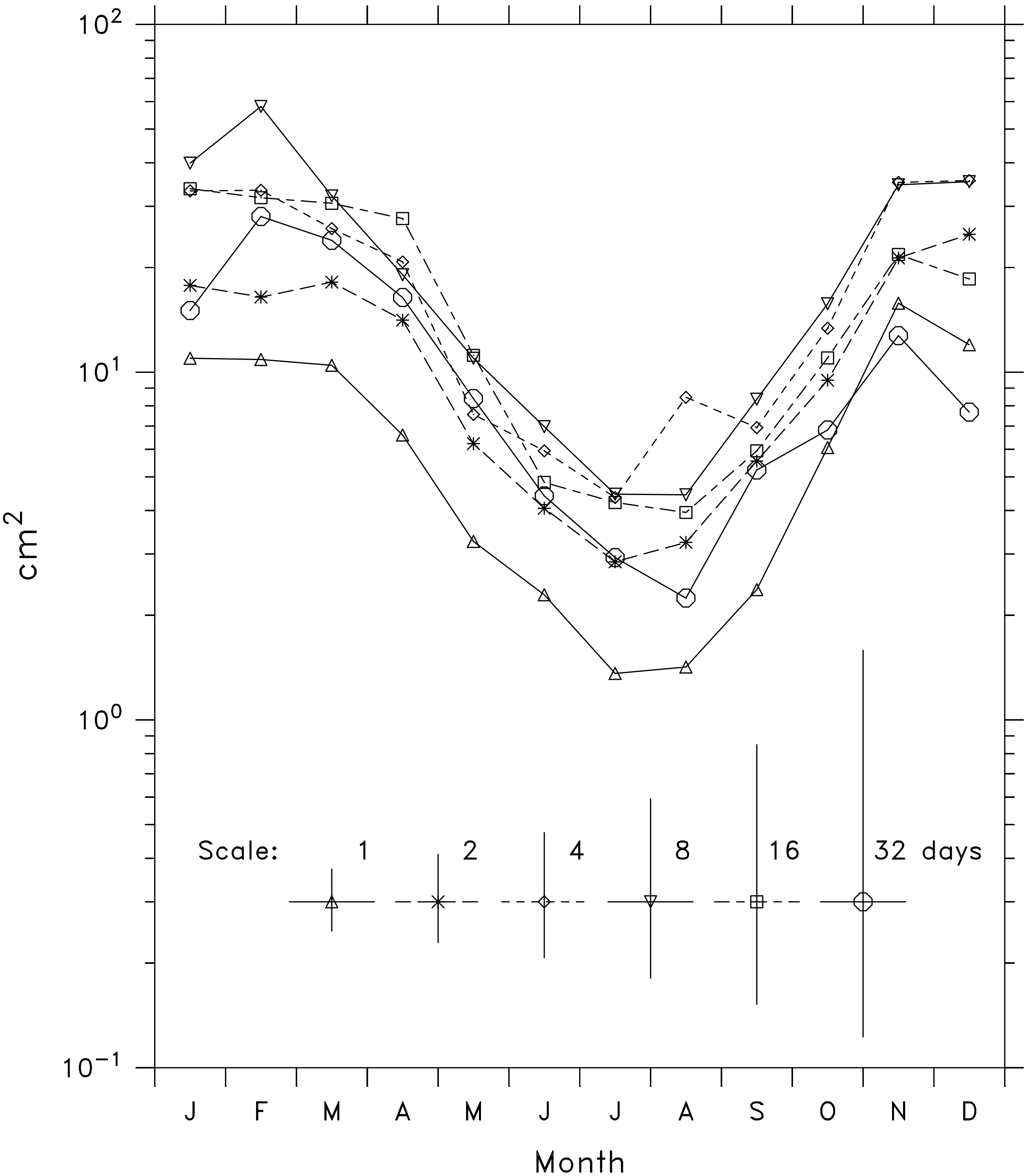

10^2
10^1
10^0
10^{-1}
cm^2
Scale: 1 2 4 8 16 32 days
J F M A M J J A S O N D
Month

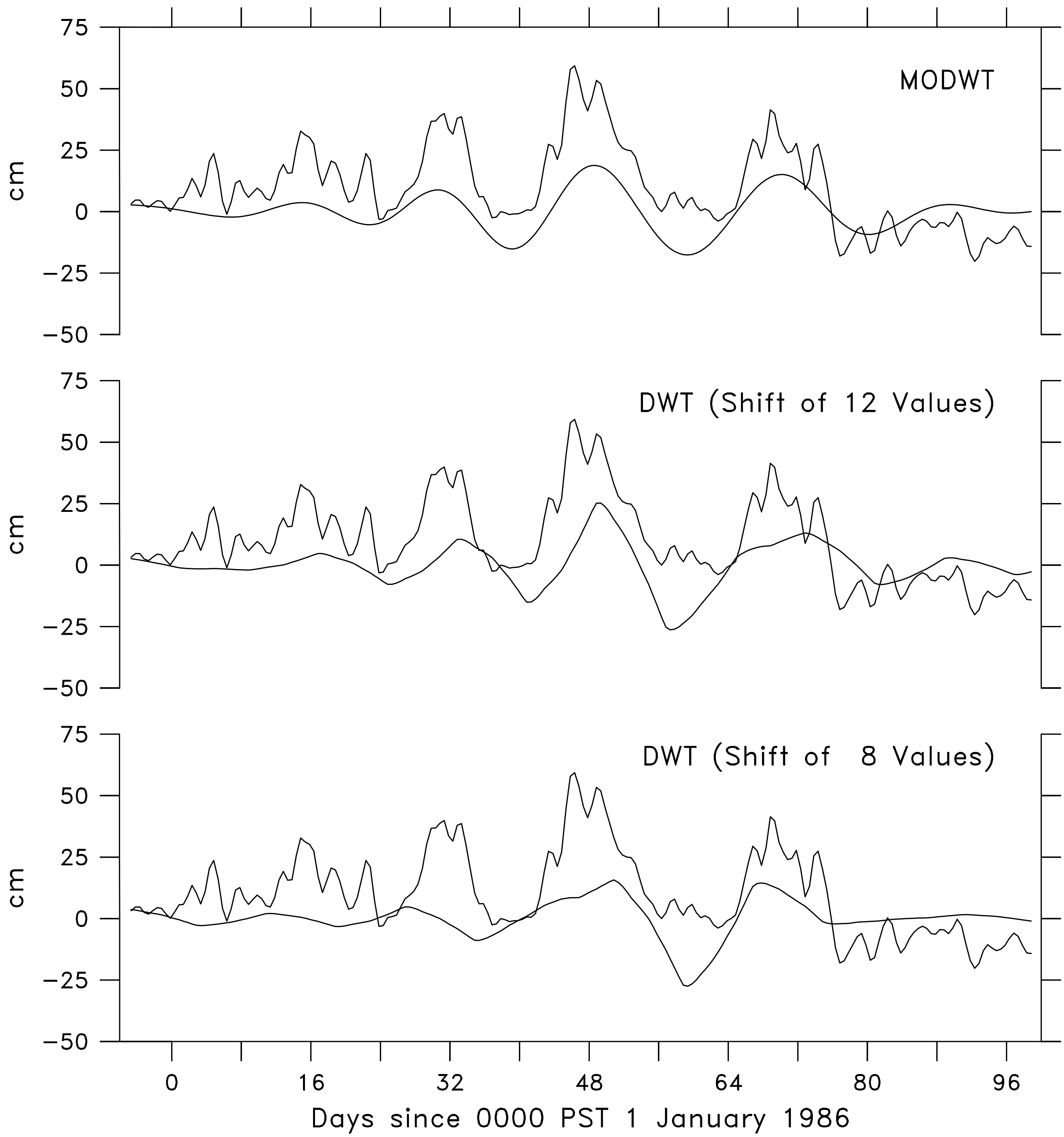
MODWT
DWT (Shift of 12 Values)
DWT (Shift of 8 Values)
cm
75
50
25
0
−25
−50
0
16
32
48
64
80
96
Days since 0000 PST 1 January 1986